# Optimizing rooftop solar PV systems in urban regions considering economic and environmental aspects

by

Nima Narjabadifam

A thesis submitted in partial fulfillment of the requirements for the degree of

Master of Science

in

Civil (Cross-disciplinary)

Department of Civil and Environmental Engineering
University of Alberta

# Abstract

In recent years, utilization of photovoltaic (PV) solar systems in built-up regions have received more attention due to global warming issues and the significance of sustainable development. The rooftops of buildings are considered highly suitable for installing PV modules to harvest solar energy and thus mitigate greenhouse gas (GHG) emissions. As a result, the use of electricity generated by rooftop PV systems, which either could meet the full or partial electricity demand of buildings or act as a distributed energy resource, is expected to contribute significantly to the sustainable development of communities. In this context, the economic and environmental perspectives of the stakeholders towards roof-installed PV systems can be critical in expanding their use, and there is a need to develop a framework for optimizing rooftop solar PV systems in urban regions considering economic and environmental aspects.

This thesis develops a search space optimization method to find the optimum layout of PV panels on roofs of buildings in urban regions, considering complicated roof shapes extracted using an advanced computer vision method. Mutual shading of PV arrays and shading impacts of objects around PV systems on the annual output and installation of PVs on roofs are also investigated. Furthermore, the optimization algorithm provides a framework to simultaneously evaluate stakeholders' economic and environmental attitudes on PV modules arrangement on roofs. Payback time (PBT) and $CO_2$ emission savings are economical and environmental criteria. Three buildings with cold climate conditions on the North Campus of the University of Alberta in Edmonton, Alberta, Canada, are investigated as case studies.

The results show the significance of stakeholders' economic and environmental perspectives on PV modules arrangement on roofs. Compared to a complete economic vision, having an

environmental concern significantly enhances annual PV system output and $CO_2$ emission savings with almost the same payback time. Furthermore, the complex shapes of roofs are also influential in choosing optimum parameters of PV systems, such as tilt angle, azimuth angle, and distances between arrays. Shading results also emphasize that not considering the shading impacts of objects around PV systems can overestimate remarkably the yearly output of PV systems. Finally, with current electricity prices and incentives considered in this study, the results show that the rooftop-installed PV projects may currently not be viable. However, applying incentives could make those projects feasible in the future.

# Preface

The study developed in the thesis has been conducted in collaboration with Dr. Mustafa Gül's research group. The model for calculating roof-installed PV systems output and optimization framework considering economic and environmental aspects in chapter three was developed by myself. The first versions of the models for obtaining 3D models from Google Maps, the rooftop segmentation/classification, the polygon approximation, the annual shading simulation, and early simulation experiments were first developed by Joseph Nofech and later improved by Asdrubal Cheng Chen and Yongquan Zhang with my collaboration. Yongquan Zhang also developed the seasonal shading analysis. Mohammed Al-Saffar generated the hourly electricity consumption data based on available data using Monte Carlo (MC) method. Finally, Michael Versteege provided the building demand data and electricity price.

A version of the part of the thesis has been published as Narjabadifam, N.; Al-Saffar, M.; Zhang, Y.; Nofech, J.; Cen, A.C.; Awad, H.; Versteege, M.; Gül, M. "*Framework for Mapping and Optimizing the Solar Rooftop Potential of Buildings in Urban Systems*," Energies 2022, 15, 1738. For that paper, I was responsible for developing the optimization framework, conducting the simulation experiments, as well as writing the manuscript. Al-Saffar, M. contributed to improving the optimization structure and computer vision formulation, helped with writing and reviewing the manuscript, and provided general guidance. Zhang, Y. contributed to enhancing various parts of the computer vision simulations and seasonal shading analysis as well as helped with writing the manuscript. Nofech, J. developed the first versions of the models for obtaining 3D models from Google Maps, the rooftop segmentation/classification, the polygon approximation, the annual shading simulation, and early simulation experiments. Cen, A.C. helped improve the earlier

versions of the models and algorithms and contributed to enhancing the computer vision algorithms and simulations. Awad, H. provided the system data and advice regarding the optimization model needs. Versteege, M. provided important discussions, perspectives, and advice on industry needs, as well as the buildings' demand data and interpretations. Gül, M. supervised this study, conceptualized the framework, acquired the funding, provided overall guidance, contributed to many fruitful discussions on the methodology, and reviewed the manuscript.

Also, a version of part of the thesis related to the combined economic and environmental impact will be submitted for publication as a journal paper in the very near future.

**Dedication**

FOR ANYONE WHO CARES ABOUT THE FUTURE OF

HUMANITY!

## Acknowledgements

**Table of Contents**

# List of Tables

# List of Figures

# CHAPTER ONE. INTRODUCTION

With increasing universal attention to global warming and efforts to reduce carbon footprints, awareness of replacing fossil fuels with clean energy and managing energy consumption in residential, commercial, and industrial sectors is increasingly expanding. Solar energy could be one of the best options for the energy management crisis among the clean energy resources due to its ubiquity and free availability [1].

In recent decades, the cost of solar photovoltaics (PV) has decreased significantly due to the pervasiveness of technology in the world. For example, PV prices have decreased about 25 times during the last two decades, from an average of 5.0 $/W in 2000 to 0.2 $/W in 2020 [2]. The impact of the price decrease can be seen in the PV installation amount, which has increased from 1 GW in 2000 to 500 GW (0.5 TW) in 2018 [3]. Also, according to the sustainable development scenario presented by the International Energy Agency (IEA), solar electricity production should reach 1940 TWh and 3268 TWh in 2025 and 2030, respectively, from 720 TWh in 2019 [4].

Buildings play a critical role in energy consumption and $CO_2$ emissions worldwide. For instance, in the United States and the European Union, buildings consume more than 40% of primary energy [5]. Moreover, buildings in the US emit 36% of $CO_2$ [6]. Rooftop mounted PV modules are among the options that can be used in buildings to cover fully or partially their energy demand. As shown in Figure 1, between 25% and 43% of the total share of installed PVs worldwide is installed on rooftops [7].
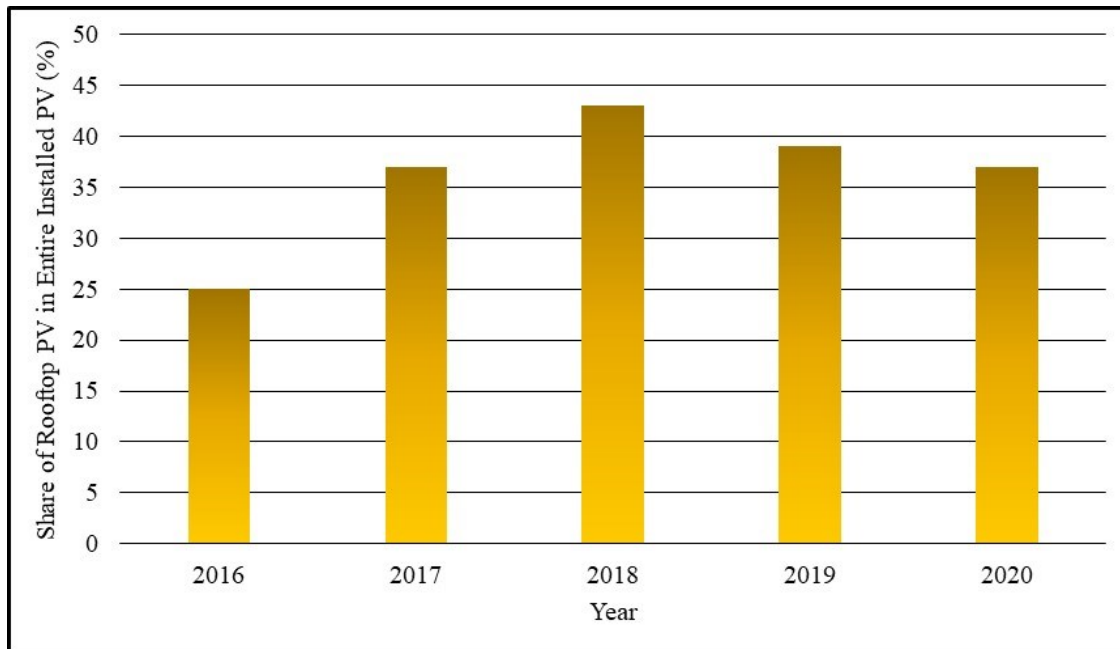
Figure 1. Share of rooftop PV installed in entire installed PV [7]

Regarding the values in Figure 1, rooftops play a critical role in solar electricity generation globally. The point to consider is that the use of rooftop PV systems in urban areas is crucial nowadays. The United Nations (UN) report states that cities play a primary role in climate change. Seventy-eight percent of global electricity consumption is related to cities, and they release more than 60 percent of GHGs while they occupy only less than two percent of Earth [8]. As a result, the use of PV systems in urban systems and their optimal use seems necessary.

Another important consideration in developing solar PV systems usage is stakeholders' vision towards them. For instance, some homeowners are interested in using PV systems for environmental benefits. In contrast, others are reluctant to invest in solar PVs due to barriers such as high initial costs or long payback times [9].

Considering the significance of rooftop-mounted PV systems, the critical role of buildings in urban systems in GHG emission, and stakeholders' attitudes toward implementing rooftop PVs arises an excellent motivation to investigate how different perspectives of decision-makers could affect the solar energy harvesting of rooftop-installed PV systems in urban regions.

## 1.1 Problem Statement and Research Objectives

Massive employment of rooftop solar PV systems in cities creates a need to automatically find the optimum solution for each building, considering the shapes of the roofs, objects on the roof, mutual shadings of buildings, and many other parameters in an automated manner. In the meantime, there has always been an emphasis on the energy production of PV systems, while valuing the solar project owners' perspectives as the main stakeholders and transforming their environmental and economic visions before implementing the project has not been appropriately considered. Thus, the current thesis develops an optimization framework to find the optimum layout of PV systems on the complex shapes of buildings' roofs in urban regions applying economic and environmental concepts of projects stakeholders.

## 1.2 Thesis Organization

The current thesis is presented in five chapters. The current chapter, which was presented as an introduction, problem statement, and general objectives, is the first chapter.

In the second chapter, a comprehensive literature review is provided to clarify the significance of the problem stated. This chapter first presents previous studies that focus on optimizing rooftop PV systems. Then, studies investigating PV systems from other aspects, such as environmental

aspects, are reviewed. Afterwards, the well-known existing tools that estimate the rooftop solar potentials are presented. Finally, this chapter is wrapped up by explaining research gaps.

Chapter three is divided into four sections. The first section explains how the information about the roofs of the buildings is extracted to be used in the optimization process. The second section describes the applied solar radiation model and the PV system output calculation details. Next, the developed optimization framework is expressed, and the economic and environmental criteria used in this thesis are defined. Finally, the last section talks about the gathering of required data.

In chapter four, roof extraction results, seasonal shading maps and optimum PV systems layout regarding economic and environmental aspects are presented and discussed for the three case study buildings. Moreover, the solar radiation model used in this thesis and the annual electricity output obtained from the developed model are validated by available resources. Finally, recommendations derived from the results are provided.

Finally, chapter five expresses the conclusion of the thesis along with its contributions and limitations. This chapter ends by providing some suggestions for future works.

# CHAPTER TWO. LITERATURE REVIEW

Various works have been conducted for evaluating rooftop-installed PV systems. The primary areas of interest of the researchers have mostly been on assessment of the rooftop PV systems in terms of energy, economics, and environment. Many studies attempted to find the best layout of PV systems in different regions to maximize the energy production of PV systems. Other works focus on investigating the viability of PV systems based on different regions' available solar radiation, the government supports, buildings demand patterns, etc. On the other hand, some studies focus on assessing the environmental benefits of using PV systems.

## 2.1    Optimization of Rooftop PV Systems

In terms of finding the optimum PV module features, e.g., tilt and azimuth angle, many studies have been carried out to find those parameters to maximize the output of PV modules and their performance. For example, El-Kassaby [10] developed an analytical and experimental model to evaluate the optimum tilt angle for south-facing solar panels in different latitudes. The author's main conclusions were that changing the tilt angle monthly results in better performance. Siraki and Pillay [11] also evaluated the optimum tilt angle in urban areas using a simple model considering a modified sky model. Their results illustrated that the three main parameters, including region latitude, climate conditions and surrounding obstacles, should be considered in finding the optimum tilt angle. In another study, Kaddoura et al. [12] found the optimum tilt angle in various cities of Saudi Arabia to maximize the solar radiation gain. They proposed that if the tilt angle of PV modules is changed in February, March, September, and October and from November to January and April to August, 99.5% of available daily solar radiation could be collected. They also pointed out that by adjusting PV modules monthly and seasonally, they could

5

gain 7.74% and 6.38% more energy compared to fixing the tilt angles. In terms of deriving an empirical equation for optimum tilt angle and latitude, Jacobson and Jadhav [13] presented the optimum tilt angle for different cities worldwide using PVWatts. Then they developed empirical correlations between optimal tilt and latitude angles for northern and southern hemispheres. Dhimish and Silvestre [14] evaluated the azimuth angle effect on the energy output of PV systems in two different locations in the UK. The results specified that over the four years if the PV modules' azimuth angles vary between −4° and +2°, the PV system generation became maximum; on the other hand, when PV panels' azimuth angle is −87°, the worst energy production occurs. Abdallah et al. [15] developed a mathematical model in MATLAB to evaluate the optimum tilt angle of south-facing panels in the United Arab Emirates. The results revealed that if the PV panels are fixed yearly at 23°, they could generate 8% more energy than installed horizontally.

In addition to the previous studies, Chang [16] used the particle-swarm optimization (PSO) method with non-linear time-varying evolution to find the optimum tilt angle of PV panels for maximizing electricity output in different cities in Taiwan. Dixit et al. [17] also used the PSO algorithm to obtain the optimum annual tilt angle. Furthermore, Talebizadeh et al. [18] found the optimum tilt and azimuth angles of PV modules in a location in Iran to maximize solar energy gain by applying the genetic algorithm (GA). In another study, Şahin [19] used optimum tilt angle data of seven cities to establish an artificial neural network (ANN) to find the optimum tilt angle in Turkey.

Apart from what has been mentioned so far, many other studies have also tried to find the optimum tilt and orientation of PV panels which references [20–23] are among them.

Finding optimal design of solar modules for the satisfaction of various objective functions is another interesting area that several researchers have studied. For instance, in terms of matching

the PV system output and building demand, Gong and Kulkarni [24] evaluated a large PV system on a rooftop to optimize the effectiveness factor that combines maximization of PV system output usage and minimization of exporting electricity to the grid. Or recently, Litjens et al. [25] investigated the impact of consumption patterns to find the optimum design of the PV system. Different objectives were studied in their research, such as self-consumption. They used Dutch data of energy consumption for commercial and residential buildings and day-ahead electricity prices of Dutch and German, considering various ratios of sales to purchase prices. They changed the azimuth angle of PVs between 75° and 285° and the tilt angle between 0° and 50°, and altogether, they evaluated 10,761 layouts. Their results clarified that in terms of maximizing the self-consumption for residential buildings, the tilt and azimuth angles should be 26° and 212°, respectively, and for commercial buildings, the optimum values are 17° and 188°, respectively. Furthermore, Awad and Gül [26] developed a generalized reduced gradient nonlinear optimization framework to define the PV system's optimal size and layout to maximize the load-match indicator. They researched the cold climate condition of Edmonton, Canada. Their results revealed that for the temperate weather regions in the northern hemisphere, a solar PV system that orients south-west and tilts $\pm 10°$ of the region latitude angle results in better self-consumption. In another study, Liu et al. [27] developed a PV systems load-matching optimization in different cities in China. They considered various parameters such as PV tilt angle, PVs' orientation, and building height to achieve zero energy building (ZEB). The PV system output potential was evaluated for both roofs and facades, considering the self-consumption and self-sufficiency of buildings. Based on their results, at least 70% of the energy needed for low-rise buildings can be supplied by the roof installed PV system in all climates of China.

Moreover, in the case of spatial analysis, Zhong and Tong [28] found the optimal spatial distance by examining the PV panels side by side alignment in order to optimize the energy output. They considered four scenarios for modules alignment, including no alignment, vertical alignment, horizontal alignment, and all alignment. The no-alignment scenario resulted in the best performance among the mentioned scenarios by increasing the maximum electricity output by up to six percent. However, their model assumed that the PV panels were parallel to the roofs. Awan et al. [29] also tried to find the optimum inter-row spacing between PV arrays to obtain the minimum Levelized cost of energy (LCOE) and maximum energy yield. They compared two PV system layouts installed on the rooftop and the ground in hot urban regions. Up to 23.7% reduction in LCOE was reported when using roof-installed rather than the ground-mounted PV system. Their results also pointed out that the optimum inter-row spacing for roof-installed and ground-mounted is 2.5 m and 1.5 m, respectively. Moreover, they concluded that using a roof-installed PV system is more beneficial than the ground-mounted system in hot areas to reduce the cooling load of building due to shading on the roof and decrease the cost of required land in urban regions. Alghamdi [30] also carried out a similar comparison between roof-mounted and ground-mount PV systems.

In another study, to enhance the existing PV system energy efficiency, Behura et al. [31] developed a new design for an existing 248 kW PV system installed on a building roof in India. They used PVsyst software to maximize the PV system's energy efficiency, resulting in saving time and money. The new design generated about 40 MWh more than the old design, and the new design had 11-13% shading loss less than the existing design. They also reported a considerable emission reduction applying the new design.

Regarding energy and economic analysis of PV systems, Freitas et al. [32], for instance, developed a multi-objective genetic model to maximize the PV system output and minimize the system cost. Ning et al. [33] used the building information model (BIM) and optimization method to automatically design a PV system to minimize the ratio of cost to power. Results revealed that the design efficiency could be enhanced up to 265% in comparison to the design of humans, and investment cost per unit of output electricity could be decreased by about 4.5%. Similar work has been carried out by Vahdatikhaki et al. [34], considering high-rise building surfaces. Korsavi et al. [35] investigated fourteen 5 kW PV systems with different arrangements, such as single array and double arrays installed on roofs in Iran's hot and dry climate. They considered the yearly energy output of systems and four economic parameters, including net present value (NPV), PBT, LCOE, and investment return. The results revealed that the single array PV system electricity generation is the maximum among all configurations while having less initial installation and wiring costs. Furthermore, they showed that the average payback is 46.9 years to 50.5 years, considering the subsidized energy tariffs. However, the average payback time is 11.6 years regarding actual electricity price. Awad et al. [36] also implemented a particle swarm optimization model to obtain the maximum electricity output of PV systems considering cost-effectiveness in different cities of Canada. Their result emphasized a tilt angle of about $\pm 5°$ of the region latitude gives the maximum energy yield. Moreover, to maximize the energy generation per roof unit area, the panels' tilt angle should be about between 0° and 10°. Combining both objectives resulted in the inter-row spacing of 1.55 m and 15.34° of tilt angle for a case study in Edmonton, Canada. In another study, Christiaanse et al. [37] developed a techno-economic optimization to specify the optimum PV system design. They used a two-level optimization and used commercial buildings in Vancouver, British Colombia, Canada, as their case study. The electricity cost of the buildings was minimized

by the lower level of the optimization model considering adjusting the fewer number of panels or energy imported from the grid. On the other hand, the upper-level model defined the PV modules' design parameters. The results pointed out that PV systems are profitable if the current cost is reduced by 50% or equal to CAD 1.25 per watt installed. Similar to previous studies, Mokhtara et al. [38] used a techno-economic evaluation to find the optimum design for rooftop PV systems for educational buildings in arid condition of Algeria. The result showed that the PV systems installed on the roofs of campus buildings are feasible both economically and technically.

## 2.2   Considering Other Aspects Such as Environmental and Social Impacts

In the continuation of the previous works, some researchers were interested in examining other aspects of using the system in addition to energy and economic analysis. To give an example, Dubey et al. [39] investigated the positive and negative socio-economic and environmental impacts of silicon-based PV modules. They pointed out reducing land use compared to conventional energy sources, reducing transmission lines, making nations less dependent on energy imports, using unutilized places such as deserts, integrating PVs to roofs and facades of buildings, and increasing environmental awareness of the community as the examples of positive socio-economic effects. On the other hand, disadvantages include competition for different land-use such as agricultural use, high initial cost, the need for energy storage for supply availability, misallocation of subsidies, and health risks during the manufacturing of the modules. Furthermore, from an environmental point of view, they mentioned the importance of recycling modules instead of producing new ones since the energy consumption during the recycling process could be reduced by more than 50% compared to the production process. Another noteworthy point is the dramatic reduction in carbon

footprint. However, they emphasized that the use of hazardous gases should be considered during the production process.

In terms of PV technologies evaluation, Perez-Gallardo et al. [40], for instance, conducted an environmental evaluation and developed a genetic algorithm to maximize the solar PV system's energy generation. The algorithm was carried out for an assumed flat rectangular-shaped surface. In addition, based on 15 objectives, including maximizing the PV system output, minimizing the payback time and energy payback time and minimizing 12 environmental factors, they studied and ranked five different solar module technologies, including the monocrystalline silicon, multi-crystalline silicon, amorphous silicon, copper indium diselenide, and cadmium telluride. Lukač et al. [41] also evaluated the economics and environmental effects of PV systems, including monocrystalline silicon (m-Si), polycrystalline silicon(p-Si), and amorphous silicon (a-Si) on the roofs of buildings using LiDAR data. First, the NPV was used for economic analysis, and the energy payback time (EPBT) and greenhouse gas emission rate were considered for environmental research. Based on Slovenia's minimum and maximum annual feed-in tariffs, the NPV of appropriate roof PV projects gets positive after three and eleven years. Then, the best economic scenario was evaluated for environmental analysis. Solar PV systems using a-Si technology were the best option among all the considered technologies from the ecological viewpoint. The best EPBT for the a-Si type PVs on roofs was about three years, while the others had greater EPBT values. However, it took the longest of all the PV technologies to get a positive NPV. Allouhi et al. [42] conducted extensive economic, energy, and environmental analyses of three different technologies in various cities of Morocco for fixed installed power of solar PV systems. The technologies included monocrystalline (m-Si), polycrystalline (p-Si), and amorphous on microcrystalline (a-Si/μc-Si). Based on energy analysis, p-Si panels perform better than the other

two types of modules. On the other hand, the discounted payback period analysis revealed that the average payback times of different cities are 17.1, 21.6, and 28.6 years for p-Si, m-Si, and a-Si/µc-Si technologies, respectively. Furthermore, the environmental analysis showed an average reduction of 1.316, 1.286, and 1.051 tons of $CO_2$ per installed kW using p-Si, m-Si, and a-Si/µc-Si, respectively. However, they did not mention the optimum layout of PV modules or the combined economic, energy and environmental impacts.

Cucchiella and D'Adamo [43] carried out a multi-criteria decision-making (MCDM) considering economic, energy, and environmental parameters to investigate the sustainability of different PV projects in Italy. Some of the criteria were EPBT, greenhouse gas per kilowatt-hour, greenhouse gas payback time, NPV, and discounted PBT. They mentioned that the main criterion in ranking the projects is the average yearly solar radiation. Sagani et al. [44] also investigated the techno-economic and environmental effects of building-integrated solar PV systems in Greece. The studied PV systems had power between 2 $kW_p$ and 10 $kW_p$. For economic analysis, results illustrated that the NPV and Internal Rate of Return increase using the larger PV system size. Furthermore, they pointed out that in the process of manufacturing and decommissioning of modules, it is evident that the larger the size of the system, the more significant the negative environmental impact. They also considered EPBT and the $CO_2$ PBT for the 9.87 $kW_p$ PV system with conventional energy systems such as diesel generators and natural gas-fired turbines. EPBT and $CO_2$ PBT based on diesel generator were 2.1 years and 1.7 years, respectively; and based on the natural gas-fired turbine was 4.1 years and 3.5 years. Therefore, they concluded that the natural gas-fired turbines usage adversely affects the PV systems' benefit to the environment. Koo et al. [45] also carried out an economic and environmental life cycle assessment to find the optimum fulfillment method of the PV systems installed on roofs to optimize the saving to investment ratio

in different cities of South Korea. The results showed that the saving to investment ratio at year 25 for Busan, Daejeon, and Seoul are 2.54, 2.485, and 2.266, respectively. The application models in their study had rectangle roofs. Recently, Gómez-Navarro et al. [46] investigated Valencia city's rooftop PV system production from a technical, economic, and environmental viewpoint. Their simulations considered four models: self-consumption, storage, selling to the grid, and net energy metering. They also studied different types of buildings such as residential single-family, commercial/industrial buildings, and public buildings. The worst-case scenario was the self-consumption model, and the best-case method was net energy metering. The payback time for commercial/industrial buildings was 3.05 and 4 years for best-case and worst-case scenarios, respectively. For the same type of buildings, yearly GHG saving was 47,310 and 40,755 tonnes for best-case and worst-case scenarios, respectively. In another study, Paudel et al. [47] assessed the economic and environmental impact of a 1 MW grid-connected PV system installed on rooftops of campus buildings in Nepal. Results illustrated that the PBT is 8.4 years, and the project's LCOE is 0.069 USD/kWh. Moreover, they mentioned that using the solar PV system decreases by 97% emission compared to the diesel generator already used on the campus. Saxena et al. [48] also evaluated the economic, energy and environmental impacts of rooftop installed PV systems in various cities of India. They considered the PV systems capacity to be 100 $kW_P$, oriented the panels to the south and fixed the tilt angle regarding the site installation location. Also, they avoided shading on panels. The results revealed that the payback time of the projects is between 5 to 6 years. They also mentioned that installing PV systems could avoid 150 to 170 tonnes of $CO_2$ emissions annually in different cities.

Yildiz et al. [49] studied the environmental impact of using polycrystalline and cadmium telluride PV modules based on data from five countries, including Germany, the US, Brazil, China, and

Japan. The results revealed that during the life cycle of one square meter of polycrystalline and cadmium telluride PV modules, 201.4 kg-$CO_2$ and 115.04 kg-$CO_2$ are emitted to the atmosphere, respectively. They also pointed out that the energy payback time for polycrystalline and cadmium telluride PV panels is 0.92 and 0.57 years, respectively.

## 2.3    Rooftop Solar Potential Estimation Tools

Many rooftop solar potential estimation tools have been developed so far. Project Sunroof is one of those tools which uses Google's data [50]. Project Sunroof takes the user's address and estimates annual serviceable sunlight hours based on daily weather conditions. It also provides information on available areas for PV modules based on analyzing the 3D model of the rooftop and surrounding trees. Also, based on the user's average monthly electricity bill, the tool estimates the PV system size [50]. The main drawback of Project Sunroof is that it works only for the United States and Puerto Rico. The other tool that could help automatically design solar PV systems on homes and commercial buildings' roofs is the SunPower Instant Design Technology [51]. The SunPower tool provides the design and estimation of savings in about 30 seconds and 60 seconds for homes and commercial buildings, respectively. The tool gets the user's address and uses artificial intelligence (AI) techniques to distinguish roof, trees, and obstructions, and then provide the solar PV design based on regional rules [51]. EnergySage® is the other tool that is powered by Google Project Sunroof. The tool calculator considers the roof size, orientation, shading, electricity prices, rebates, incentives, and market price data to estimate the solar potential of roofs of the given address and the savings [52]. Again, the main drawback is that it works only for addresses inside the US, and it seems that the layout of a PV system is not provided. The next tool is Mapdwell which estimates the solar potential of roofs based on a 3D elevation analysis of buildings besides considering

regional weather conditions and obstacles, and other structures around the investigated building. The regional cost and incentives are regarded in the evaluation [53]. The tool gives the technical report such as system size, the number of panels, annual output, and roof area usage, financial reports like total system cost, payback time, net present value, monthly and yearly savings, and other impacts like carbon offset, and carbon capture [53].

Another tool based on Google Research named Open Buildings provides footprints of buildings on the ground. However, this tool is not for solar applications but applications such as population estimation and urban planning. This tool outlines buildings in a polygonal format through deep learning and high-resolution satellite images[54]. From installing solar panels viewpoint, it will be limited due to the lack of obstacles on the roof and the details of the roofs.

Moreover, some studies tried to evaluate the solar potential of roofs using airborne LiDAR and orthophoto [55] or photogrammetry from unmanned aerial vehicles (UAVs) [56]. Fuentes et al. [56] also mentioned other studies in their research that have conducted the solar radiation analysis using geographic information systems (GIS) techniques.

## 2.4   Research Gap

Regarding the literature review, considerable research gaps exist. To the best of the author's knowledge, almost no study has considered the simultaneous impact of the owners' economic and environmental perspectives on the arrangement of PV panels in roof-mounted solar PV projects. Another main limitation of previous studies is that they do not consider complex roof shapes while optimizing PV system features such as tilt and azimuth angles. In practice, the roofs usually have obstacles, and their shapes are not necessarily rectangular. Also, the roof of a building could be segmented into different flat or sloped parts. Without automation of extracting roofs, it is hard to

evaluate PV system performance on any arbitrary roofs of buildings. However, some commercial tools are available, such as Google Sunroof and SunPower, they are not available to all countries, including Canada, and they do not provide a layout in all applications, and if they do, they will not necessarily provide optimal layout based on building consumption criteria, economic and environmental criteria, and even a combination of them. Finally, most of the previous work provided shadow modelling on panels with less detail and, in some cases, without shading analysis.

Due to the research gaps mentioned in the previous paragraph, the current thesis presents a comprehensive study for the optimum installation of PV systems on buildings' roofs, especially commercial and educational buildings, as follows:

- Optimizing the arrangement of PV panels on the roofs by considering buildings' electricity load and stakeholders' economic and environmental visions.

- Using the search space optimization technique regarding the nonlinear nature of the problem in relation to control parameters such as tilt angle and azimuth angle and complicated shapes of roofs containing irregular-shaped obstacles.

- Analyzing the mutual shading of PV arrays on each other in addition to the shading impacts of objects around PV systems such as neighbouring tall buildings, high rooftops in the building under investigation, chimneys, trees, large HVAC systems, and parapets.

# CHAPTER THREE. METHODOLOGY

This chapter presents the proposed methodology. First, it will elaborate on the roof extraction methods from 3D building models. Next, the solar radiation model implemented in this study will be presented in detail, considering shading impacts. Then, the developed optimization framework, including defining control variables, economic and environmental factors and their combined effect, and the objective function, will be discussed. Finally, the chapter will conclude with the data collection section.

## 3.1    Roof Extraction

The first step in determining the optimal arrangement of rooftop-installed PV panels and their output is to determine the roof shapes in detail. The information needed to install the panels can be obtained using buildings' 3D models and image processing to extract roof shapes with details. Details about the methodology since the early development can be found in Nofech et al. [57] and Narjabadifam et al. [58].

### 3.1.1    3D Model of the Buildings & 2D Heightmap

It is necessary to know the spatial distances on the roofs to get accurate information. However, Google's 3D models do not provide precise information about distances for analysis. Therefore, a process is required to convert the 3D model of the building into a 2D model of the heightmap.

In the first step, a single three-dimensional frame of the building is taken using RenderDoc, an open-source graphic debugger [59]. In the next step, the 3D model captured from RenderDoc is converted to a .stl format using Blender, an open-source 3D graphic software [60], and with the aid of an add-on called "Maps Models Importer" [61]. Finally, the 3D model with the .stl format

17

is converted into a 2D height map used to distinguish the roofs of a building with different elevations.

Figure 2 to Figure 4 represent Google's 3D models for the three case study buildings in this thesis: Administration Building (ADMIN), Cameron Science, Engineering, Business Library Building (CAM), and Earth and Atmospheric Sciences Building (EAS), respectively [62].



Figure 2. Google's 3D model of the ADMIN building. Imagery ©2021 Google, Imagery ©2021 Maxar Technologies, Map data ©2021
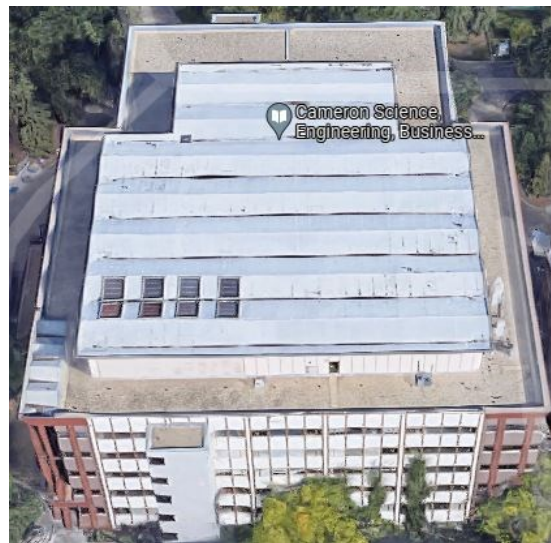


Figure 3. Google's 3D model of the CAM building. Imagery ©2021 Google, Imagery ©2021 Maxar Technologies, Map data ©2021

Figure 4. Google's 3D model of the EAS building. Imagery ©2021 Google, Imagery ©2021 Maxar Technologies, Map data ©2021

Another issue is converting the arbitrary scale of the 3D model of the buildings to its actual values. This problem is solved using the specific scaling tool of Google Maps and selecting two points on the two-dimensional map.

The use of Google's 3D maps, given their accuracy and availability for buildings, makes the present study's algorithm effective for all residential, commercial, educational, and even industrial buildings. However, in the absence of Google's 3D model for buildings in a specific region, LiDAR devices are needed to extract the roofs. Therefore, the present study relies only on the 3D models available by Google's 3D maps.

### 3.1.2   Roof Identification

A pixel-based algorithm is used to identify different roofs of a building. In order to distinguish a roof from the rest of the map, it needs to be separated by an edge resulting from a sharp difference in height. The edge is identified when the slope between two adjacent pixels exceeds 45 degrees. Roofs are defined when they are at least 3.5 meters above the ground and have enough space to install at least one standard PV module, considering the walkway around it. Using the roof identification algorithm, the building heightmap can be separated into distinct regions with their height span and slope. Each of those particular regions is called a blob [63].

19

If the slope connecting two flat regions is less than 45 degrees, the previous edge detection is failed. To overcome the mentioned issue, a percentile analysis is applied to check the considerable height difference in the heightmap of each blob. Figure 5 represents an example of percentile analysis for a blob. The x-axis is the percent grade or rank of pixels heights, and the y-axis is the height percentile of each percent grade. In the example, 40 percent of the hypothetical roof has a height of 14m, 20 percent between 14m and 16m, and the remaining 40 percent is 16m. Based on percentile analysis, a flat surface is defined as a surface in which the rate of increase of height percentile is less than 0.17/25 (m/%). The mentioned threshold value has been obtained empirically. Accordingly, a one-dimensional array, $i_{flat}$, is defined as follows:

$$i_{flat} = \begin{cases} 1, & \left(\dfrac{\boldsymbol{v}_i - \boldsymbol{v}_{i-1}}{2.5} < \dfrac{0.17}{25}\right) | \left(\dfrac{\boldsymbol{v}_{i+1} - \boldsymbol{v}_i}{2.5} < \dfrac{0.17}{25}\right) \\ 0, & otherwise \end{cases} \qquad (1)$$

where $v$ is the vector of height percentile value. The regions with $i_{flat}$ zero values are eliminated from the map, which means that those zero values separate the map.
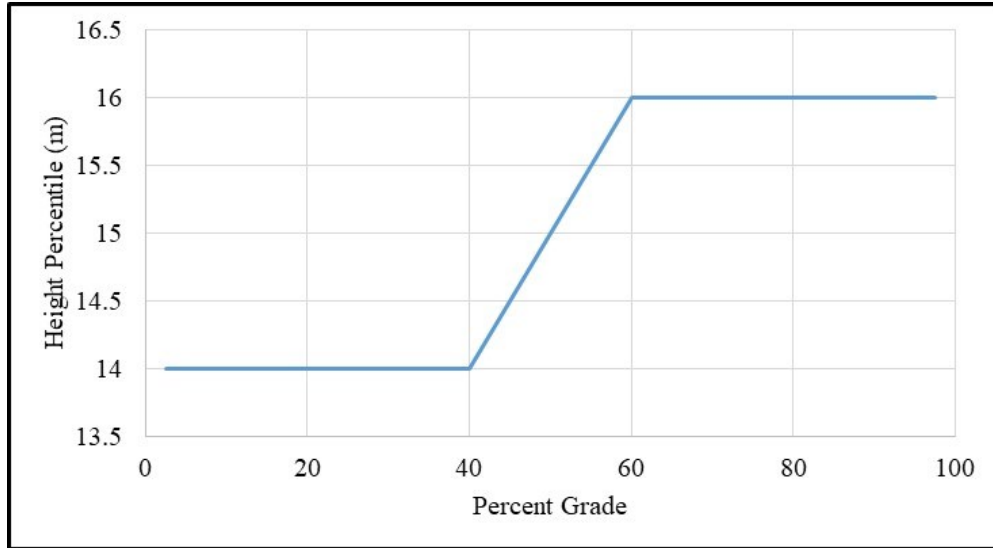


Figure 5 An example of percentile analysis for a blob heightmap

20

### 3.1.3  Roof Classification

After identifying potential rooftops of a building, they should be examined in detail and classified for the next steps. In this level, the area of each roof, roof slope, the orientation of the roof to east or west, and a few other properties are specified.

A rooftop with a relatively fixed slope could be considered for PV installation; however, the curved shape or any irregular-shaped roof is not a good option for installing PV modules because of installation issues. Therefore, an individual rooftop with approximately constant height is classified as "flat," and a roof with a roughly fixed slope is categorized as "slanted." Finally, any roof not part of the above categories is classified as "irregular."

The first step in the classification step is to check each of the individual rooftops to see whether it is flat. The percentile analysis of the particular roof heightmap is evaluated with 2.5% steps to investigate the flatness. Similar to the blob separating rule mentioned in Eq. (1), at least 50% of the roof points must have a height change of less than 0.17/25 (m/%), and at least 10% of the roof points must be ultra-flat, meaning have the rate of increase of height percentile less than 0.05/25 (m/%).

In the next step, any roof that is not flat is checked to see whether it falls into the slanted category or not by using a plane fitting to the heightmap. Suppose the standard deviation of the height difference between the blob's heights and the fitting plane is less than 0.095 m. In that case, the roof is classified as "slanted"; otherwise, the roof falls into the "irregular" category. The slanted roof properties such as slope and direction relative to the north are specified from the fitting plane properties.

The other issue is identifying the multiple slanted roofs with a zero or close to zero height difference at the intersection of the two roofs, such as hip, gable, or butterfly roofs. These roofs have so far been classified as "irregular." Thus, an enhanced splitting algorithm is used to separate roofs of those irregular ones into smaller parts [64–66]; for instance, a gable roof is separated into two slanted roofs with specific slopes. The ridge that separates blobs and belongs to both should be found to overcome the issue. Figure 6 represents an example of a butterfly roof and how a low ridge is located on a heightmap. As shown in Figure 6b, a linear morphological element is used to find the local maxima or minima moving over various directions. All pixels' height units are in meters in Figure 6. Each time, an equal and consecutive number of map pixels are isolated and compared to the number of segments in the linear element. Suppose the mid-segment of the linear morphological element matches the smallest height of the pixels in question. In that case, a value of "1" is assigned to that pixel in a binary map. The binary table shown in Figure 6c will be obtained if the procedure is repeated in all directions. As a result, consecutive numbers of "1" in the binary map can divide an irregular classified roof into two individual roofs to check their slantedness.

The procedure described so far was for finding a low ridge. The whole heightmap had to be multiplied by (-1) to find a high ridge like a gable roof. In this case, the low ridge located in the reverse map will equal the high ridge in the actual map.

a)

| $x_{-2}$ | $x_{-1}$ | $x_0$ | $x_1$ | $x_2$ | | | |
|----|----|----|----|----|----|----|----|
| 14 | 13 | 12 | 11 | 10 | 11 | 12 | 13 |
| 14 | 13 | 12 | 11 | 10 | 11 | 12 | 13 |
| 14 | 13 | 12 | 11 | 10 | 11 | 12 | 13 |
| 14 | 13 | 12 | 11 | 10 | 11 | 12 | 13 |
| 14 | 13 | 12 | 11 | 10 | 11 | 12 | 13 |
| 14 | 13 | 12 | 11 | 10 | 11 | 12 | 13 |
| 14 | 13 | 12 | 11 | 10 | 11 | 12 | 13 |
| 14 | 13 | 12 | 11 | 10 | 11 | 12 | 13 |

| 0 | 0 | 0 | 0 | 1 | 0 | 0 | 0 |
|---|---|---|---|---|---|---|---|
| 0 | 0 | 0 | 0 | 1 | 0 | 0 | 0 |
| 0 | 0 | 0 | 0 | 1 | 0 | 0 | 0 |
| 0 | 0 | 0 | 0 | 1 | 0 | 0 | 0 |
| 0 | 0 | 0 | 0 | 1 | 0 | 0 | 0 |
| 0 | 0 | 0 | 0 | 1 | 0 | 0 | 0 |
| 0 | 0 | 0 | 0 | 1 | 0 | 0 | 0 |
| 0 | 0 | 0 | 0 | 1 | 0 | 0 | 0 |

(b)                                                                                      (c)

Figure 6. Obtaining ridge a) hypothetical butterfly roof, b) morphological element and heightmap of a roof, c) binary map of ridge

### 3.1.4  Polygon Approximation

After classifying the roofs, the roof shapes need to be simplified for PV installation. In fact, in this stage which is the final step of roof analysis, a 2D binary figure of a roof will be transformed into continuous coordinates, which are the corners of an approximate polygon of the roof. Then,

depending on how much the polygon matches roof shape edges, a score is calculated for the roof obtained as:

$$Confidence = \frac{\sum_{i=1}^{pixels\ in\ the\ map} polygon\ map\ score(i) \times roof\ map\ score(i)}{total\ number\ of\ enteries\ of\ 1.0\ in\ the\ roof\ map} \qquad (2)$$

Each pixel is assigned a point so that "1.0" corresponds precisely to a roof's edges, and as pixels are farther from the edge on both sides, the score decreases gradually. On the other hand, a straight line is drawn in the estimated polygon map from one corner to the other. Thus, the pixels that correspond to the estimated line are filled with "1". Figure 7a schematically shows a small part of the map of a roof, including one edge between two corners. Figure 7b represents polygon approximation for the same small part. In Figure 7a, it is assumed that the "1"s in the first and last columns illustrate the corners of one of the roof edges.

| 0.5 | 0.5 | 0.6 | 0.6 | 0.5 | 0.5 | 0.5 | 0.5 | 0.5 | 0.6 | 0.6 | 0.6 | 0.6 | 0.6 | 0.6 | 0.5 | 0.5 |
|---|---|---|---|---|---|---|---|---|---|---|---|---|---|---|---|---|
| 0.6 | 0.6 | 0.7 | 0.7 | 0.6 | 0.6 | 0.6 | 0.6 | 0.6 | 0.7 | 0.7 | 0.7 | 0.7 | 0.7 | 0.7 | 0.6 | 0.6 |
| 0.7 | 0.7 | 0.8 | 0.8 | 0.7 | 0.7 | 0.7 | 0.7 | 0.7 | 0.8 | 0.8 | 0.8 | 0.8 | 0.8 | 0.8 | 0.7 | 0.7 |
| 0.8 | 0.8 | 0.9 | 0.9 | 0.8 | 0.8 | 0.8 | 0.8 | 0.8 | 0.9 | 0.9 | 0.9 | 0.9 | 0.9 | 0.9 | 0.8 | 0.8 |
| 0.9 | 0.9 | 1.0 | 1.0 | 0.9 | 0.9 | 0.9 | 0.9 | 0.9 | 1.0 | 1.0 | 1.0 | 1.0 | 1.0 | 1.0 | 0.9 | 0.9 |
| 1.0 | 1.0 | 0.9 | 0.9 | 1.0 | 1.0 | 1.0 | 1.0 | 1.0 | 0.9 | 0.9 | 0.9 | 0.9 | 0.9 | 0.9 | 1.0 | 1.0 |
| 0.9 | 0.9 | 0.8 | 0.8 | 0.9 | 0.9 | 0.9 | 0.9 | 0.9 | 0.8 | 0.8 | 0.8 | 0.8 | 0.8 | 0.8 | 0.9 | 0.9 |
| 0.8 | 0.8 | 0.7 | 0.7 | 0.8 | 0.8 | 0.8 | 0.8 | 0.8 | 0.7 | 0.7 | 0.7 | 0.7 | 0.7 | 0.7 | 0.8 | 0.8 |
| 0.7 | 0.7 | 0.6 | 0.6 | 0.7 | 0.7 | 0.7 | 0.7 | 0.7 | 0.6 | 0.6 | 0.6 | 0.6 | 0.6 | 0.6 | 0.7 | 0.7 |

(a)

| 0 | 0 | 0 | 0 | 0 | 0 | 0 | 0 | 0 | 0 | 0 | 0 | 0 | 0 | 0 | 0 | 0 |
|---|---|---|---|---|---|---|---|---|---|---|---|---|---|---|---|---|
| 0 | 0 | 0 | 0 | 0 | 0 | 0 | 0 | 0 | 0 | 0 | 0 | 0 | 0 | 0 | 0 | 0 |
| 0 | 0 | 0 | 0 | 0 | 0 | 0 | 0 | 0 | 0 | 0 | 0 | 0 | 0 | 0 | 0 | 0 |
| 0 | 0 | 0 | 0 | 0 | 0 | 0 | 0 | 0 | 0 | 0 | 0 | 0 | 0 | 0 | 0 | 0 |
| 0 | 0 | 0 | 0 | 0 | 0 | 0 | 0 | 0 | 0 | 0 | 0 | 0 | 0 | 0 | 0 | 0 |
| 1.0 | 1.0 | 1.0 | 1.0 | 1.0 | 1.0 | 1.0 | 1.0 | 1.0 | 1.0 | 1.0 | 1.0 | 1.0 | 1.0 | 1.0 | 1.0 | 1.0 |
| 0 | 0 | 0 | 0 | 0 | 0 | 0 | 0 | 0 | 0 | 0 | 0 | 0 | 0 | 0 | 0 | 0 |
| 0 | 0 | 0 | 0 | 0 | 0 | 0 | 0 | 0 | 0 | 0 | 0 | 0 | 0 | 0 | 0 | 0 |
| 0 | 0 | 0 | 0 | 0 | 0 | 0 | 0 | 0 | 0 | 0 | 0 | 0 | 0 | 0 | 0 | 0 |

(b)

Figure 7. Schematic of polygon approximation for one edge of a shape a) roof map scores b) polygon map score

The confidence score varies between zero and one. The closer the score to one, the better the approximated polygon matches the outlines of the roof edges.

## 3.2    Solar Radiation Model

The solar radiation model of the PV system tries to find the hourly electricity generation by the PV system for each building. To establish the solar radiation model, first, the following definitions are presented.

- *Extraterrestrial Radiation ($G_{ext}$)* is the solar radiation at the top edge of Earth's atmosphere, which theoretically is the superior boundary of available solar radiation on a horizontal surface on the Earth [67].

- *Beam Radiation* is the radiation that a PV module receives directly from the sun without any atmosphere scattering effect [67].

- *Diffuse Radiation* is a part of the solar radiation that a PV module gets after scattering by the atmosphere [67].

- *Reflected Radiation* is the part of the radiation that a PV module receives after being reflected by the ground [67].

- *Incidence Angle ($\theta$)* is the angle between the normal to the PV module and beam radiation [67].

- *Zenith Angle ($\theta_z$)* is the angle between the solar beam and vertical line [67].

- *Declination Angle ($\delta$)* is the angle between the axis of rotation of the Earth and the equator, which varies between -23.45° and 23.45° [67].

- *Latitude ($\phi$)* is the angular location of the installed PV panel, which varies between -90° and 90°, and positive values represent north hemisphere regions [67].

- *Module's Azimuth Angle* ($\gamma$) is the angle between the projection of the module's normal on the horizontal surface and the local meridian plane, which varies between -180° and 180°. The orientation to the south is zero, negative values are toward the east, and positive values are toward the west [67].

- *Hour Angle* ($\omega$) is the sun's angular displacement about the local meridian plane. Based on the Earth's rotation about its axis, every 15 degrees is equal to one hour. The morning times are negative, and the afternoon times are positive [67].

- *Module's Tilt Angle* ($\beta$) is the angle between the PV module and horizontal surface, varying between 0° and 180° [67].

- *Solar Altitude Angle* ($\alpha_s$) is the angle between solar rays and horizontal lines, which complement the zenith angle [67].

- *Solar Azimuth Angle* ($\gamma_s$) is the angle between the projection of solar rays on the horizontal surface and south. The east-south side is negative, and the west-south side is positive [67].

Note that all angle units are in degrees, and radiation units are in $W/m^2$. Three buildings investigated in this study (ADMIN, CAM, and EAS buildings) are located at the North Campus of the University of Alberta in Edmonton, Alberta, Canada, with geographical coordinates of Edmonton being 53.5461° N 113.4938° W.

After defining the required parameters and angles, the solar radiation model could be set up. The total clear-sky solar radiation ($G_{cs}$) that a surface receives is defined as in Eq. (3) [67]:

$$G_{cs} = G_{beam} + G_{diff} + G_{refl} \tag{3}$$

To calculate the first and third components of Eq. (3), first, the clear-sky global horizontal radiation $(G_{GH})$ needs to be defined as in Eq. (4)[68,69]:

$$G_{GH} = 0.7 \times G_{ext} \times \cos(\theta_z) \tag{4}$$

Using $(G_{GH})$, the beam radiation can be found as in Eq. (5):

$$G_{beam} = G_{GH} \times \frac{\cos\theta}{\cos\theta_z} \tag{5}$$

The ratio in Eq. (5) is a geometric coefficient that converts the radiation on the horizontal surface to the inclined one. The angle of incidence defined previously can be calculated as in Eq. (6) [67]:

$$\theta = \cos^{-1}(\sin\delta\,\sin\phi\,\cos\beta - \sin\delta\,\cos\phi\,\sin\beta\,\cos\gamma + \cos\delta\,\cos\phi\,\cos\beta\,\cos\omega$$
$$+ \cos\delta\,\sin\phi\,\sin\beta\,\cos\gamma\,\cos\omega + \cos\delta\,\sin\beta\,\sin\gamma\,\sin\omega) \tag{6}$$

In Eq. (6), if the surface tilt angle is set to be zero, the zenith angle can be calculated as in Eq. (7) [67]:

$$\theta_z = \cos^{-1}(\sin\delta\,\sin\phi + \cos\phi\,\cos\delta\,\cos\omega) \tag{7}$$

The third component of Eq. (3), reflected radiation, can be obtained as in Eq. (8) [67]:

$$G_{refl} = \rho_g \times G_{GH}\left(\frac{1 - \cos\beta}{2}\right) \tag{8}$$

where $\rho_g$ is the ground reflectance, and the ratio represents the surface-to-ground view factor. The second term in Eq. (3) also could be found as in Eq. (9) [26,70]:

$$G_{diff} = \left[14.29 + 21.04 \left(\frac{\pi}{2} - \theta_z \times \frac{\pi}{180}\right)\right] \left(\frac{1 + \cos\beta}{2}\right) \qquad (9)$$

Where the first term inside the brackets defines the diffuse radiation on the horizontal surface, and the second term inside the parathesis $\left(\frac{1+\cos\beta}{2}\right)$ represents the surface-to-sky view factor.

The value calculated so far are based on clear-sky assumptions. To obtain the actual power ($G$) at the module location, it is necessary that $G_{cs}$ is multiplied by the clear-sky index as in Eq (10):

$$G = k_t \times G_{cs} \qquad (10)$$

Eq. (10) considers the impact of sky cloudiness on the electricity generation of the PV module.

Apart from the clear-sky index that can affect PV electricity generation, shading cast on PV modules could be the other crucial factor that can be considered. PV generation can suffer from two types of shading effects: 1) adjacent PV arrays and 2) surrounding objects such as buildings, trees, HVAC equipment, roofs, chimneys, etc.

### 3.2.1 Mutual Shading of Adjacent PV Arrays

Figure 8 shows the three rows of PV modules, which the last two rows being shaded by their front rows. To calculate the height of the shading ($L_s$) on the PV module at the adjacent row, Eq. (11) could be used [71]:

$$L_s = L_m \times \left(1 - \frac{\frac{L_{ir}}{L_m} + \cos\beta}{\cos\beta + \frac{\sin\beta\cos(\gamma_s - \gamma)}{tg\,\alpha_s}}\right) \qquad (11)$$

where $L_{ir}$ is the inter-row spacing and $L_m$ is the length of the panel, as shown in Figure 8.
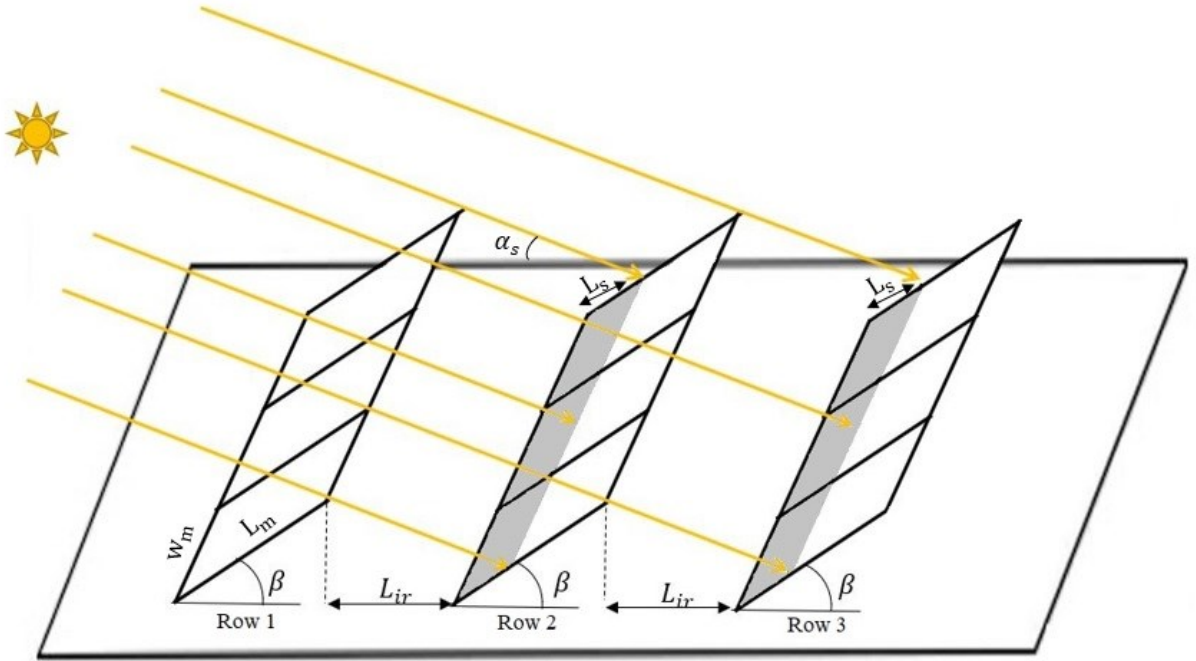
Figure 8. Mutual shadings of adjacent PV rows

Note that Eq. (11) considers the entire orientation of the panels and the sun's location in the sky. It is also important to note that in this study, it was assumed that even if only one of the module cells were under shading, all cells in the same row of the module would lose their performance to generate electricity. For this reason, the shadow length on the adjacent row will be equal to the width of the module. It is also assumed that if a portion of cell height is shaded, the shading length will be modified to a new length ($L'_s$) as in Eq. (12):

$$L'_s = L_s + reminder(L_s, cell_{size}) \tag{12}$$

where $cell_{size}$ is the standard size of the PV cell [72]. Using Eq.(12), a partially shaded PV module cell is considered fully shaded.

### 3.2.2 Obstacles Shading Effects

Objects around the solar PV systems can partially or entirely overshadow the modules. As a result, shading analysis of objects around the PV panels will be necessary to find their impacts on PV modules placement and electricity generation. Obstacles that can block sunlight and cast shadows on ceilings could be tall buildings, trees, HVAC equipment on the roofs, chimneys, or even elevated roofs on the same building. The first step is to find how much of each region of rooftops is shaded during the year. A shading map of the building and surrounding area would be helpful to reach this goal. Figure 9 could help to find if any pixel on the shading map at a specific day moment is shaded or not.
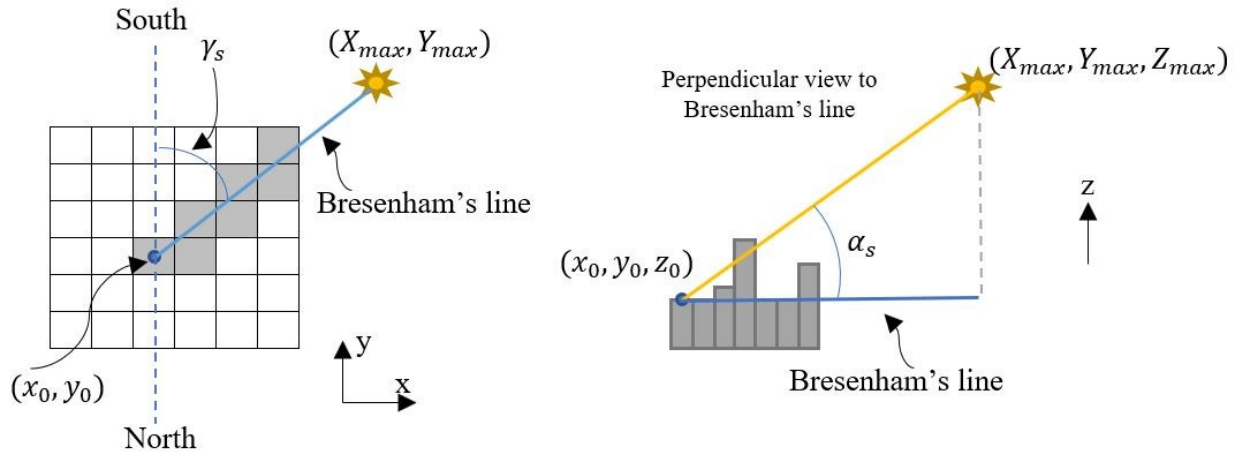


Figure 9. Schematic of assigning brightness scores for each pixel at a specific moment

A line, Bresenham's line, is drawn on the 2D surface in the direction of sun rays projection to the horizontal surface connecting the reference point $(x_0, y_0, z_0)$ to the projection of a point on the sun rays line on the XY plane outside the map. The line equation based on Bresenham's line algorithm is written as in Eq. (13) [73]:

$$[x_p, y_p] = bresenham[(x_o, y_o), (X_{max}, Y_{max})] \tag{13}$$

where, $x_p$ and $y_p$ are the pixel components of a vector pointing from $(x_o, y_o)$ to $(X_{max}, Y_{max})$. Note that $x_p$ and $y_p$ are discretized integer values assigned to each pixel. Using Bresenham's line algorithm, the pixels along Bresenham's line path are determined (gray pixels in Figure 9). Finally, if even in one of (x, y) coordinates on the line, the height of the pixel $(h_p)$ is greater than the z component of the line connecting the reference point and $(X_{max}, Y_{max}, Z_{max})$, then the reference pixel would be shaded. The same procedure could be done for other pixels on the map to examine if they are also shaded or not.

The average brightness score in a specific period of time could be defined as in Eq. (14):

$$br_{score} = \frac{\sum_{i=1}^{operating\ hours} b_i}{Sum\ of\ annual\ operating\ hours} \tag{14}$$

where $b$ is a Boolean value and could get two values, zero or one. At the specific moment, if the pixel is shaded, $b$ equals zero, and if the pixel is not shaded, $b$ equals one. Based on Eq. (14), $br_{score}$ could be calculated for each hour, day, month, season, or year.

Next, based on where the solar panels are located in the shading map, they are evaluated to what extent they are shaded. To do this, pixels enclosed in the PV module are identified, and their average score is calculated. The obtained average score will be the brightness score of that module. Figure 10 demonstrates the schematic of how the average brightness score is calculated for PV panels. Each of the PV panels encompasses six pixels, which by averaging those six brightness scores, the final brightness score for the left and right modules are obtained 0.8 and 0.72, respectively.

| 0.35 | 0.50 | 0.65 | 0.65 | 0.65 | 0.65 | 0.65 | 0.65 |
| 0.50 | 0.65 | 0.65 | 0.75 | 0.75 | 0.75 | 0.65 | 0.65 |
| 0.75 | 0.75 | 0.75 | 0.75 | 0.75 | 0.75 | 0.65 | 0.50 |
| 0.85 | 0.85 | 0.85 | 0.85 | 0.75 | 0.65 | 0.65 | 0.35 |
| 0.95 | 0.95 | 0.85 | 0.75 | 0.75 | 0.65 | 0.50 | 0.25 |
| 1.00 | 0.95 | 0.85 | 0.75 | 0.65 | 0.50 | 0.25 | 0.15 |
| 0.95 | 0.85 | 0.75 | 0.65 | 0.50 | 0.35 | 0.05 | 0.00 |

Figure 10. Schematic of two PV modules and brightness scores of pixels

The brightness scores of all panels in the PV system are averaged, resulting in a coefficient ($br_{\text{score,avg}}$) that applies the surrounding obstacles' shading impact on the PV system electricity generation. This study assumes that if the coefficient, named as brightness threshold, is less than 0.6, the PV panel is dismissed from the PV system. Also, note that the average brightness score is calculated based on useful working hours, so the shading impacts of obstacles in the morning and evening that can exaggerate the average brightness score are removed. However, even though getting an average brightness score based on operating hours around noon could still overestimate the brightness score, it dramatically decreases computation time and yields the worst-case scenario.

### 3.2.3 PV System Electricity Generation

Regarding shading effects, the PV system electricity generation during the year is calculated as in Eq. (15):

$$G_{\text{PV system}} = br_{\text{score,avg}}$$
$$\times \sum_{h=1}^{\text{operating hours}} \left( G(h) \times t \times L_{\text{m}} \times w_{\text{m}} \times num_{\text{unshaded}} \times \eta/1000 \right. \tag{15}$$
$$\left. + G(h) \times t \times L_m \times w_m \times num_{\text{shaded}} \times \frac{L_{\text{m}} - L'_{\text{s}}}{L_{\text{m}}} \times \eta /1000 \right)$$

where $\eta$ is the PV panel efficiency. Also, $num_{\text{unshaded}}$, and $num_{\text{shaded}}$ outline the number of unshaded and shaded PV modules in the PV system, respectively, due to mutual shading of PV arrays. $L_{\text{m}}$ and $w_{\text{m}}$ are the length and width of the modules, respectively, and $L'_s$ is the modified shadow length due to the mutual shading effect of PV arrays. In Eq. (15), $t$ represents the time interval for calculating the electricity generation, which in this study is one hour.

Note that another factor affecting annual electricity production is the snow factor. According to the four-year data of the practical study conducted by the Northern Alberta Institute of Technology (NAIT), the production reduction was measured 0.25%, 0.81%, 1.73%, 4.04%, 4.70%, and 4.47% for tilt angles of 90°, 53°, 45°, 27°, 18°, and 14°, respectively [74]. However, since for higher tilt angles (around and above the studied location), the snow factor loss is less than 2%, the effect of snow coverage is neglected in the current study.

## 3.3 Optimization Framework of Solar PV System Layout

Installing PV modules on rooftops could be observed from different viewpoints, mainly economic or environmental. The optimum layout for a PV system on the roofs of buildings could be completely different if the goal is changed. However, the other way is to look at the problem from the lens of both parameters at the same time, i.e., economic-environmental. In other words, we can look at the problem from the perspective of MCDM.

Many constraints are crucial in investigating the optimum PV system layout and amount of output energy. The first type of constraint is related to spatial characteristics, including roof space, obstacles on the roof, shapes of roofs, and distances between rows of PV modules. The second type is related to the PV panels, such as their technology type, efficiency, or at what angles to the ground or south are installed. Finally, the other limitation is the grid interaction of those grid-connected PV systems, which could disturb the grid voltage. However, in this study, the investigated buildings' demands are higher than the PV system output, and thus this limitation is not considered. Furthermore, various assembly and service companies provide different PV system settings. Therefore, it is inevitable that based on selecting assembly and service companies, the choice of panels, inverters, cables, and other items could be different. Considering all those items requires a complete database of those products, and adding them to the model will dramatically complicate the optimization model and increase computational time. Thus, one specific product is chosen for the optimization problem in this study. Among the variables mentioned above, three variables, including panels' tilt ($\beta$) and azimuth ($\gamma$) angles and inter-row spacing ($L_{ir}$) are considered as control variables in this research.

The following subsections will present economic and environmental parameters and their combination in the optimization framework. Finally, the optimization framework itself will be provided.

### 3.3.1 Defining Economic Parameter

Among the economic parameters such as payback time, net present value, internal rate of return, etc., the payback time is considered for evaluation in this study. The payback time is the needed period when the future cash inflow compensates for the project's investment. Therefore, if the

payback time is shorter, the project is deemed more economically viable. The payback time method

has been used in several studies, such as [75–77], to examine the feasibility of the investment in

PV systems.

Initial cost and annual revenue are two crucial factors required in finding the payback period. The

initial cost ($IC$) or initial investment is defined as in Eq. (16):

$$IC = C_w \times num \times P_{nom} \tag{16}$$

where $C_w$ is the price per installed Watt of PVs ($/W), $num$ is the number of PVs in the installed

system, and $P_{nom}$ is the nominal power of the PV modules. To find the annual revenue earned by

using the PV system, first, the hourly revenue ($Rev_h$) is calculated as in Eq. (17):

$$Rev_h = \begin{cases} (G_h - D_h) \times E_{\text{sell},h} + D_h \times E_{purchase,h}, & G_h > D_h \\ G_h \times E_{\text{purchase},h} \quad , & G_h \leq D_h \end{cases} \tag{17}$$

where $G_h$ is the hourly output of the PV system and $D_h$ is the hourly electrical demand of the

building. Moreover, the cost of electricity purchased from the grid is denoted by $E_{purchase,h}$ and

the price at which electricity is sold to the grid is denoted by $E_{\text{sell},h}$. According to Eq. (17), if the

hourly electricity generation of the PV system is greater than the hourly demand, two types of

benefits can be observed; first, the cost saved for purchasing the entire demand from the grid

supplied by the PV system. The second is the amount of money that comes from selling surplus

electricity to the grid. On the other hand, if the PV system output is less than the building demand,

the benefit equals the money saved for not buying part of the load provided by the PV system.

Finally, adding up all the hourly revenues for a year, the annual revenue is calculated as

($Rev_{annual}$) in Eq. (18):

$$Rev_{annual} = \sum_{i=1}^{annual\ operating\ hours} Rev_h\ (i) \tag{18}$$

A similar method for calculating the annual benefit was carried out by Theault et al. [78]. The electricity cost is assumed to be constant during the time the analysis is done. The degradation of PV panels is also considered negligible; hence, the annual revenue should be consistent in all years of investigation. The equivalent present value (EPV) of yearly revenues is obtained using uniform series of cash flows [79] as in Eq. (19):

$$EPV = Rev_{annual}\left[\frac{(1+i)^n - 1}{i(1+i)^n}\right] \tag{19}$$

where $i$ is the interest or discount rate that considers the money's time value, and $n$ is the year in which the time value of the annual revenue is converted to the present time. In the present study, the annual maintenance cost is neglected [75].

At the final stage, the payback time could be calculated using Eq. (20) and solving it for $n$:

$$IC - EPV = IC - Rev_{annual}\left[\frac{(1+i)^n - 1}{i(1+i)^n}\right] = 0 \tag{20}$$

### 3.3.2   Defining Environmental Parameter

The environmental parameter addressed in this study is the $CO_2$ emission saving by generating electricity with solar PV systems instead of coal-fired power plants. About 1000 grams (1.01 kg) of carbon dioxide equivalent is emitted to the atmosphere per one kilowatt-hour of electricity generation in coal-based power plants [80,81]. Also, based on life cycle assessment, 201.4 kg-$CO_2$ equivalents are emitted to the atmosphere per square meter of polycrystalline PV modules [49]. As a result, the $CO_2$ emission saving (kg-$CO_2$) of a PV system for this study is defined as in Eq. (21):

$$CO_2 \text{ emission saving } = +G_{PV\ system} \times N_{op} \times 1.01 - num \times Area_{PV} \times 201.4 \qquad (21)$$

where $G_{PV\ system}$ is the annual electricity generation of the PV system, $N_{op}$ is the operational years of PV panels which are usually 20 or 25 years, *num* is the number of PV modules in the system, and $Area_{PV}$ is the area of a PV panel.

### 3.3.3   Economic and Environmental Combined Impact

After defining economic and environmental parameters in the last two sub-sections, the combined impact of both parameters is now defined. Based on each layout of a PV system, a payback time and $CO_2$ emission saving amount could be calculated. In order to be able to compare the effect of both parameters simultaneously, we first make both parameters dimensionless. For this purpose, first, the minimum possible payback time and the maximum $CO_2$ emission saving are calculated for the different arrangements of the PV system panels. Then the combined impact of both parameters for any arrangement of PV panels in the system is defined as an index in Eq. (22):

$$\begin{aligned} Ind_{eco-env}&(\beta, \gamma, L_{ir}) \\ &= a \times \frac{minimum\ payback\ time}{payback\ time(\beta, \gamma, L_{ir})} \\ &+ b \times \frac{CO_2 emission\ saving(\beta, \gamma, L_{ir})}{maximum\ CO_2\ emission\ saving} \end{aligned} \qquad (22)$$

where each fraction is a number between zero and one. The coefficients *a* and *b* also consider the importance of each of these economic and environmental parameters by the project owner or any project-related stakeholders. Note that the summation of *a* and *b* always should be one. Each layout with a specific $\beta, \gamma$, and $L_{ir}$ is considered as an alternative in the decision-making process. Since the scope and focus of the research are not mainly on the MCDM process and algorithms, the simplest method is carried out by applying weights to the criteria and ranking the alternatives. Regarding Eq. (22), the closer the $Ind_{eco-env}$ to one, the more economically and environmentally

efficient the project is. In this research, five states of decision-makers' opinions on modules arrangement in the PV system is evaluated as follows:

- 100% economic attitude and ignoring environmental factors ($a = 1, b = 0$),

- 75% economic attitude and 25% environmental attitude ($a = 0.75, b = 0.25$),

- The same weight for both economic and environmental parameters ($a = 0.5, b = 0.5$),

- 25% economic attitude and 75% environmental attitude ($a = 0.25, b = 0.75$),

- 100% environmental attitude and ignoring economic factors ($a = 0, b = 1$).

### 3.3.4   Optimization Framework

This study considers three variables, including PV modules tilt and azimuth angles and inter-row spacing, to find the optimum layout regarding the objective function. The search space optimization algorithm is used since the problem is nonlinear, and due to the irregular shapes of roofs, a direct relation between roof and PV system dimensions cannot be specified. The same method also has been used by Litjens et al. [25]. The research space is discretized by five degrees for tilt and azimuth angles and half-meter inter-row spacing. The following sub-section defines the objective function. Note that the *a* and *b* coefficients in Eq. (22) also should be determined by the project stakeholders.

The objective function, maximizing the economic and environmental impacts simultaneously, is defined as in Eq. (23):

$$Maximize\ Ind_{eco-env}(\beta, \gamma, L_{ir}) \tag{23}$$

Subject to

$$
\begin{aligned}
&0° \leq \beta \leq 85°; \qquad \text{if a roof is flat} \\
&-90° \leq \gamma \leq 90°; \qquad \text{if a roof is flat} \\
&1m \leq L_{ir} \leq 4.5m\ ; \qquad \text{if a roof is flat} \\
&L_{ir} = 0\ and\ \beta = roof's\ slope, \gamma = roof's\ orientation\ ; \qquad \text{if a roof is slanted}
\end{aligned} \tag{24}
$$

Regarding the constraints for flat roofs, panels' tilt angle changes from horizontal to almost vertical mode, and their orientations change in the east-south-west direction. For inter-row spacing, the minimum one-meter distance is considered between PV arrays. The upper limit of inter-row spacing is also approximately based on the shadow length of the PV panels occurring at the winter solstice. Note that PVs' tilt, azimuth, and inter-row spacing only change if installed on flat roofs. For sloped roofs, PV modules are mounted parallel to the slanted rooftops and without any distance between arrays. That means that the tilt angle of PVs is the same as the slope of the slanted roofs, and their orientation is similar to the building's orientation.

## 3.4   Data Collection

It is vital to consider atmospheric parameters such as air temperature and the cloudiness of the sky to calculate the PV panel output correctly. In general, the efficiency of crystalline PV panels decreases by about 0.5% for a one degree Celsius increase from the standard test conditions (STC) temperature [82]. Given that the buildings under study are located in Edmonton with cold climate conditions, the ambient temperature effect in this study has been neglected. However, the impact of sky cloudiness is considered. Clear-sky index ($k_t$) values for each minute for the year 2016 are obtained from Awad and Gül [26]. $k_t$ minutely values are averaged to find the hourly values because the solar radiation model in the present study is hourly-basis.

The present work uses the properties of one of the PV module products manufactured by CandadianSolar; some of its essential features are presented in Table 1 [83]. In terms of the initial cost analysis presented in Eq. (16), the installation cost per watt is needed to be specified. The installation cost is considered \$2.80 per watt based on the information from the Energy Management and Sustainable Operations (EMSO) at the University of Alberta. The cost of electricity purchased from the grid, $E_{purchase,h}$, in Eq. (17) is the other factor should be defined. Based on the information provided by the EMSO of the University of Alberta, the purchasing price is, on average, \$0.1015/kWh applied for all hours of the year in this study. The electricity price sold to the grid, $E_{sell,h}$, for small micro-generators, those whose capacity is up to 150 kW, is the same as, $E_{purchase,h}$ [84]. The other parameter is the interest rate in Eq. (19), which is assumed to be 2.2% based on the Government of Alberta interest rate benchmark [85].

Table 1. PV module properties [83]

| **Properties** | |
| --- | --- |
| Cell Type | Poly-crystalline |
| Nominal Maximum Power | 400W |
| Module Efficiency | 18.1% |
| Length | 2108 mm |
| Width | 1048 mm |
| Temperature Coefficient | -0.36 % / °C |

Finally, the last data required is the electricity demand of the building under consideration, which again is obtained from the EMSO at the University of Alberta. The monthly electricity consumption data are available for all buildings in addition to one month's hourly electricity consumption data of one building. Using the available hourly data and ratio of monthly consumption of buildings, the Monte Carlo (MC) method is applied to generate hourly electricity

consumption of buildings. Figure 11, for instance, shows the hourly electricity load profile for three buildings based on the MC simulation in March 2019.
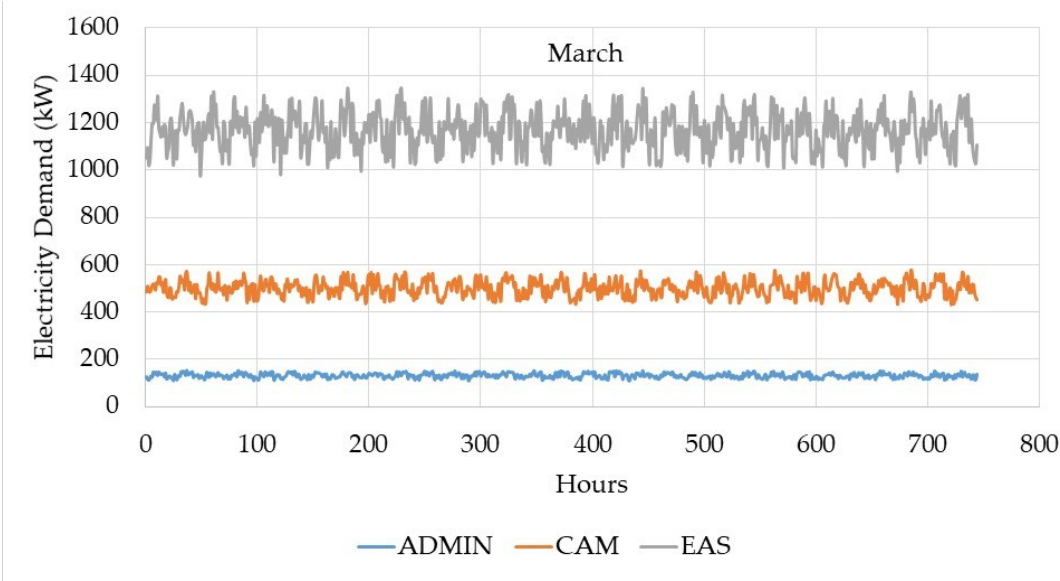


Figure 11. Electricity demand profile of three investigated buildings in March 2019

# CHAPTER FOUR. RESULTS AND DISCUSSIONS

In this chapter, the results obtained using the proposed methodology on the case study buildings (ADMIN, CAM, and EAS buildings) will be presented. First, the roof extraction results will be discussed. Then, the shading maps of ADMIN, CAM, and EAS buildings are provided based on considering existing surrounding and roof objects. The next step will validate the solar radiation model and annual electricity generation. Finally, the optimization results for different states of MCDM will be provided and discussed.

## 4.1 Roofs Extraction Results

As mentioned in the "Roof Extraction" sub-sections in the previous chapter, the first step is obtaining a 2D heightmap of investigated buildings. Figure 12 to Figure 14 show the top view of the buildings and 2D corresponding heightmaps. In the heightmaps, dark blue and dark red regions respectively represent the map's minimum and maximum heights. The numbers in the colour bar represent the heights in pixels.
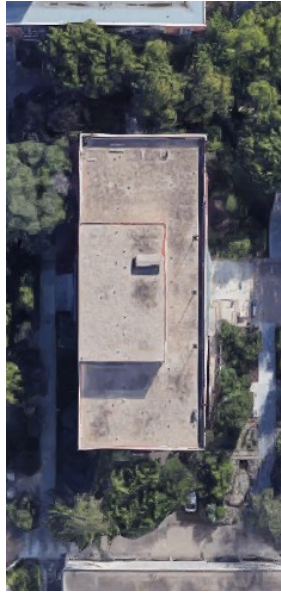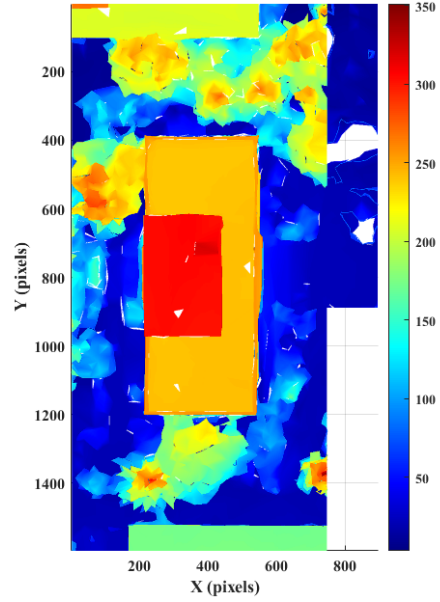
(a)                    (b)

Figure 12. a) Bird's-eye view of Google's 3D model b) 2D heightmap model of the ADMIN building. Imagery ©2021 Google, Imagery ©2021 Maxar Technologies, Map data ©2021



(a)                    (b)

Figure 13. a) Bird's-eye view of Google's 3D model b) 2D heightmap model of the CAM building. Imagery ©2021 Google, Imagery ©2021 Maxar Technologies, Map data ©2021

(a)                                                                                  (b)
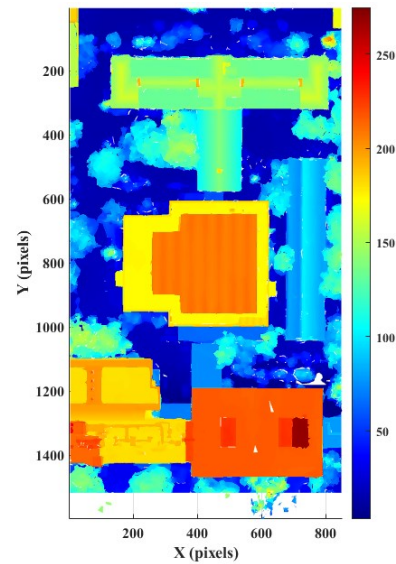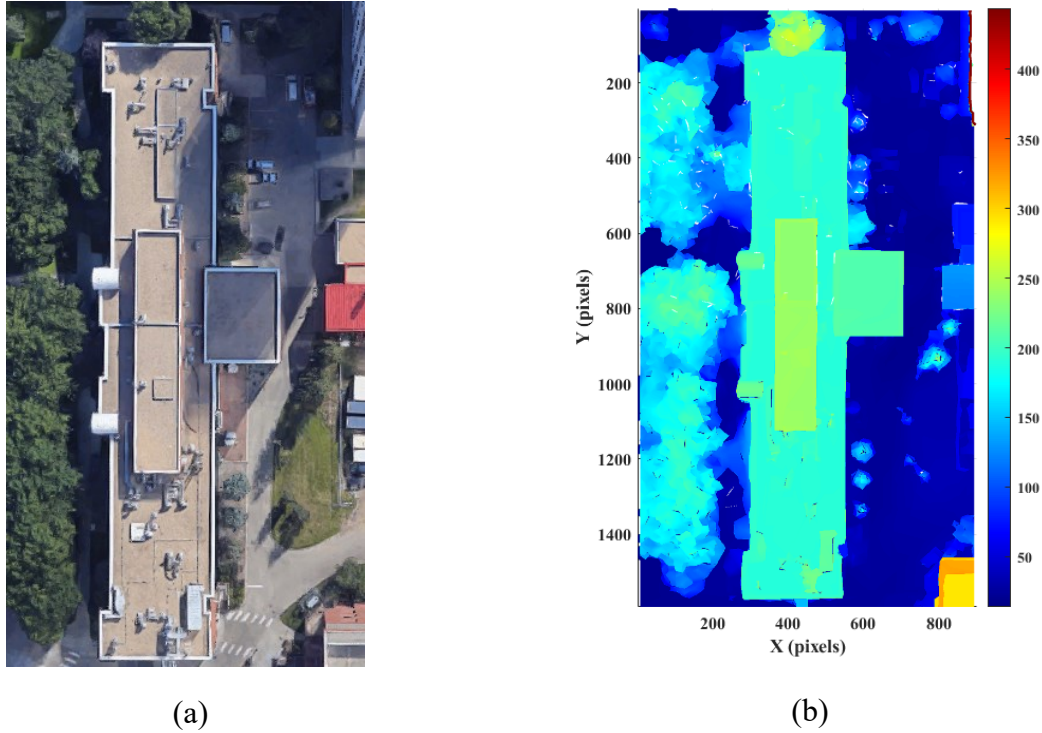
Figure 14. a) Bird's-eye view of Google's 3D model b) 2D heightmap model of the EAS building. Imagery ©2021 Google, Imagery ©2021 Maxar Technologies, Map data ©2021

Elevation of roofs in pixels and almost accurate capturing of roofs' shapes are clearly observable in Figure 12 to Figure 14. The dark blue in the maps is considered as ground. Smooth surfaces like flat roofs are the same colour, but a combination of different colours represents uneven surfaces like trees. The different elevations of roofs in ADMIN and CAM buildings are clearly defined.

Figure 15 to Figure 17 demonstrate the identified and classified roofs of ADMIN, CAM, and EAS buildings, respectively. Regarding Figure 15, the ADMIN building only has two flat roofs, marked in blue, with relatively simple shapes. On the other hand, CAM building contains all three types of roofs: flat, slanted, and irregular. As shown in Figure 16, the fourteen slanted roofs, shown as green, in the center of the CAM building are surrounded by the only flat roof. In addition, a small irregular roof, specified by red, is observable in the lower-left corner. It can also be shown that

there are no considerable obstacles on CAM roofs. Finally, as shown in Figure 17, the EAS

building has a few flat roofs with three irregular ones.
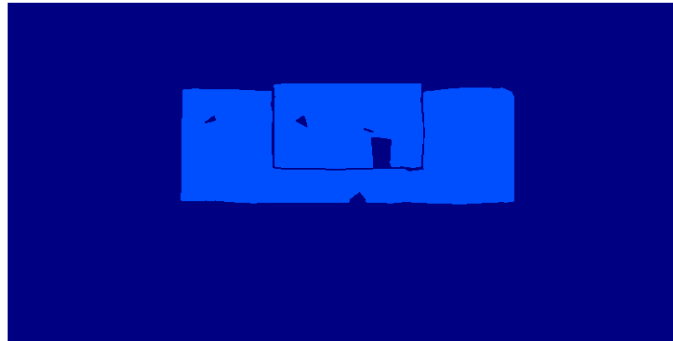


flat
slanted
irregular
Figure 15. Identified and classified roofs of ADMIN
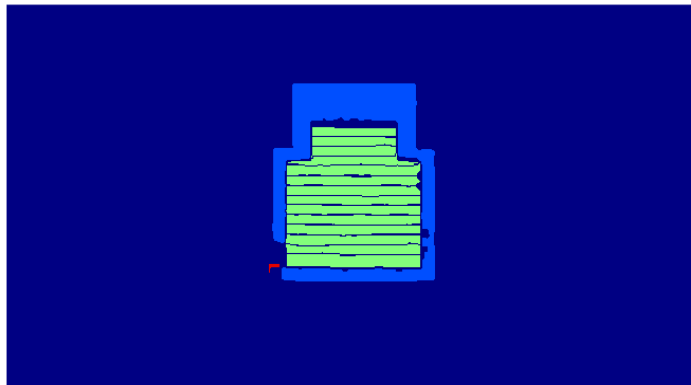


flat
slanted
irregular
Figure 16. Identified and classified roofs of CAM
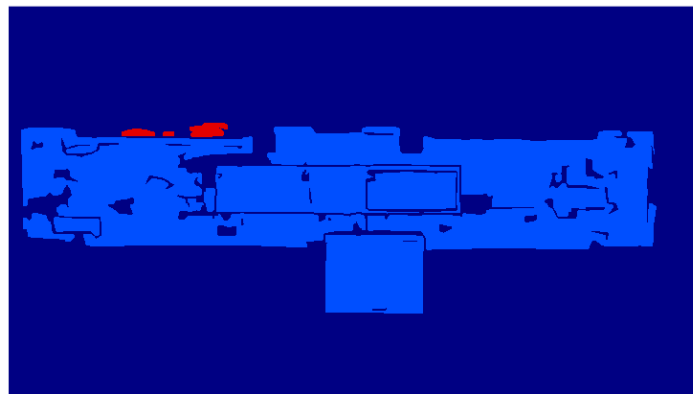


flat
slanted
irregular
Figure 17. Identified and classified roofs of EAS

Furthermore, Table 2 represents the confidence scores of those mentioned roofs for all three buildings based on polygon approximation, and Figure 18 to Figure 20 shows the three buildings' roofs IDs. The rooftops that are classified as irregular obtain zero confidence scores. Another noteworthy point is that the more regular and uncomplicated the shape of the roofs, the higher their score. For instance, roof number 15 in the CAM building, the northmost slanted roof, is very close to a rectangular shape, so the confidence score is close to 1.0.

Table 2. Confidence scores for ADMIN, CAM, and EAS roofs

| Roof ID | Confidence Scores | | |
|---|---|---|---|
| | ADMIN | CAM | EAS |
| 1 | 0.702 | 0.785 | 0.770 |
| 2 | 0.806 | 0.851 | 0.823 |
| 3 | --- | 0.808 | 0.835 |
| 4 | --- | 0.845 | 0.909 |
| 5 | --- | 0.816 | 0.837 |
| 6 | --- | 0.835 | 0.731 |
| 7 | --- | 0.851 | 0.902 |
| 8 | --- | 0.876 | 0.846 |
| 9 | --- | 0.821 | 0.000 |
| 10 | --- | 0.826 | 0.000 |
| 11 | --- | 0.867 | 0.000 |
| 12 | --- | 0.903 | --- |
| 13 | --- | 0.849 | --- |
| 14 | --- | 0.849 | --- |
| 15 | --- | 0.949 | --- |
| 16 | --- | 0.000 | --- |
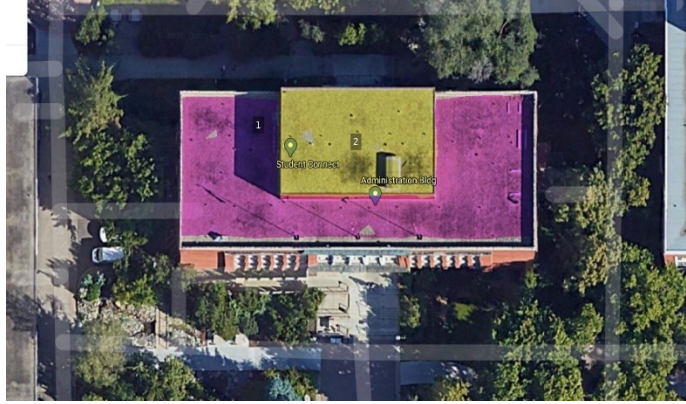
Figure 18. Rooftop IDs of ADMIN. Imagery ©2021 Google, Imagery ©2021 Maxar Technologies, Map data ©2021



Figure 19. Rooftop IDs of CAM. Imagery ©2021 Google, Imagery ©2021 Maxar Technologies, Map data ©2021
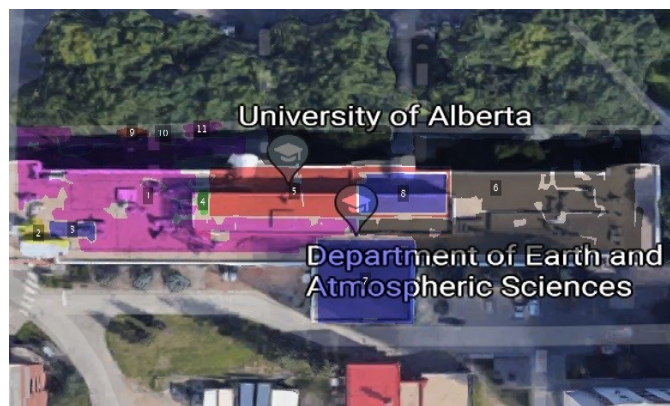


Figure 20. Rooftop IDs of EAS. Imagery ©2021 Google, Imagery ©2021 Maxar Technologies, Map data ©2021

## 4.2   Obstacles Shading Around PV System

Knowing how much each roof area is shaded helps effectively calculate PV system output.  The shadow on the roofs could be cast either by surrounding objects such as tall buildings and trees or objects inside the target building such as elevated roofs, chimneys, parapets, and large HVAC systems. The seasonal shading maps showing brightness scores of pixels for the ADMIN, CAM, and EAS buildings, are illustrated in Figure 21 to Figure 23, respectively. The Spring season starts from the March Equinox and ends in the June Solstice, which is also the summer starting day. The September Equinox is the summer end day and the beginning of the autumn. Autumn ends in the December Solstice, which is the start of winter. Finally, winter's last day is the March Equinox. ADMIN, CAM, and EAS buildings are identified with yellow boxes, and the only taller building around the target buildings is specified by the red box, which is near the EAS.

As can be seen in the following figures, the darker pixels are abundant in autumn and winter, which is predictable since the shading length of objects is longer in those seasons than in spring and summer.

a. Spring                 b. Summer
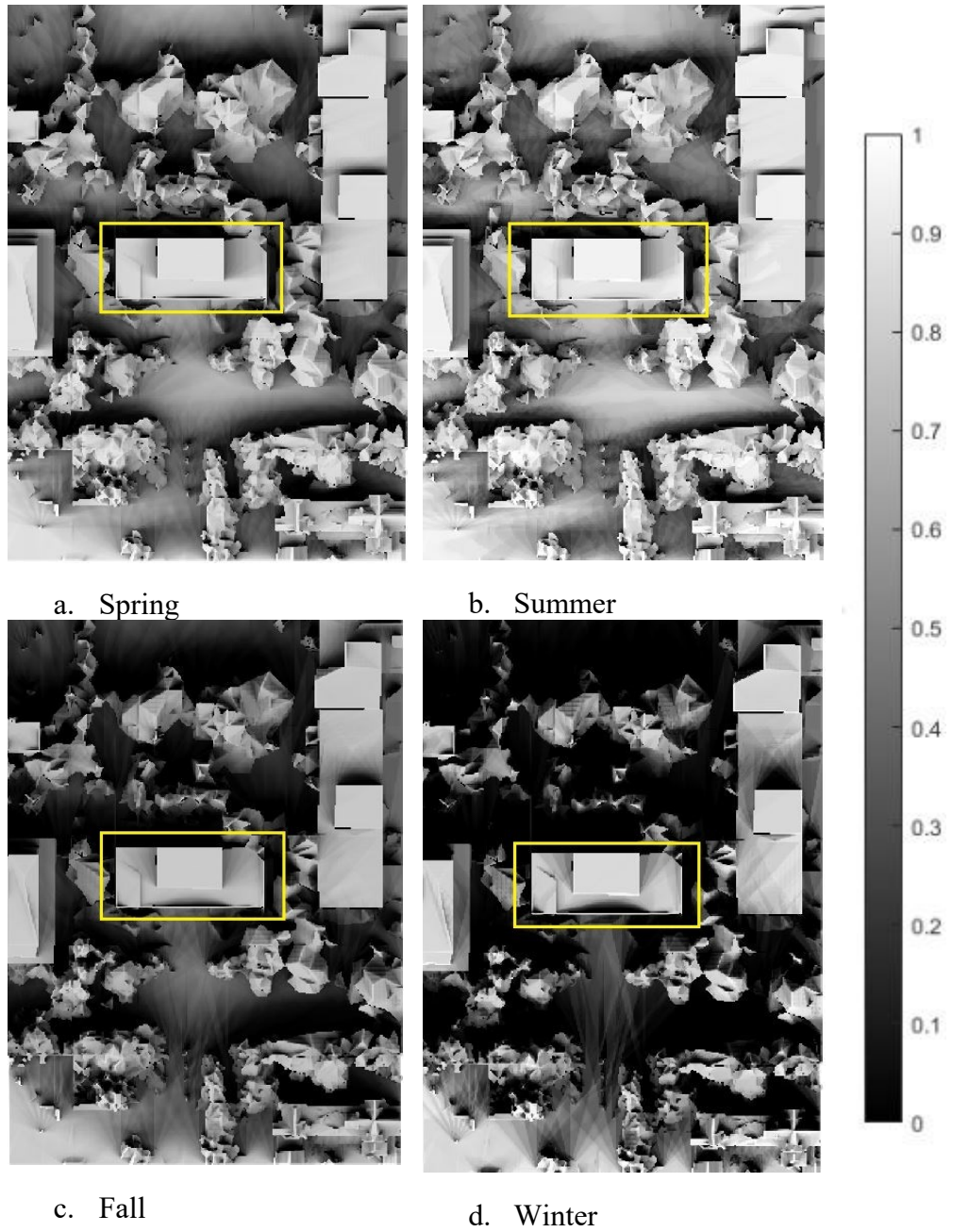
c. Fall                 d. Winter

Figure 21. Shading map of the ADMIN building at a) spring, b) summer, c) fall, and d) winter
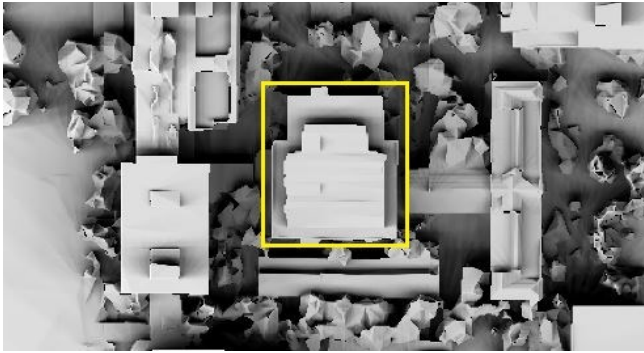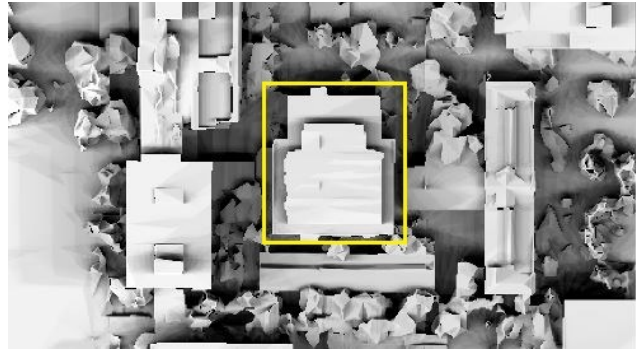
a. Spring     b. Summer
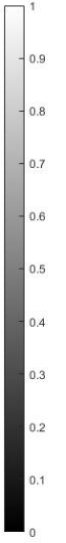
c. Fall     d. Winter

Figure 22. Shading map of the CAM building at a) spring, b) summer, c) fall, and d) winter

a. Spring      b. Summer
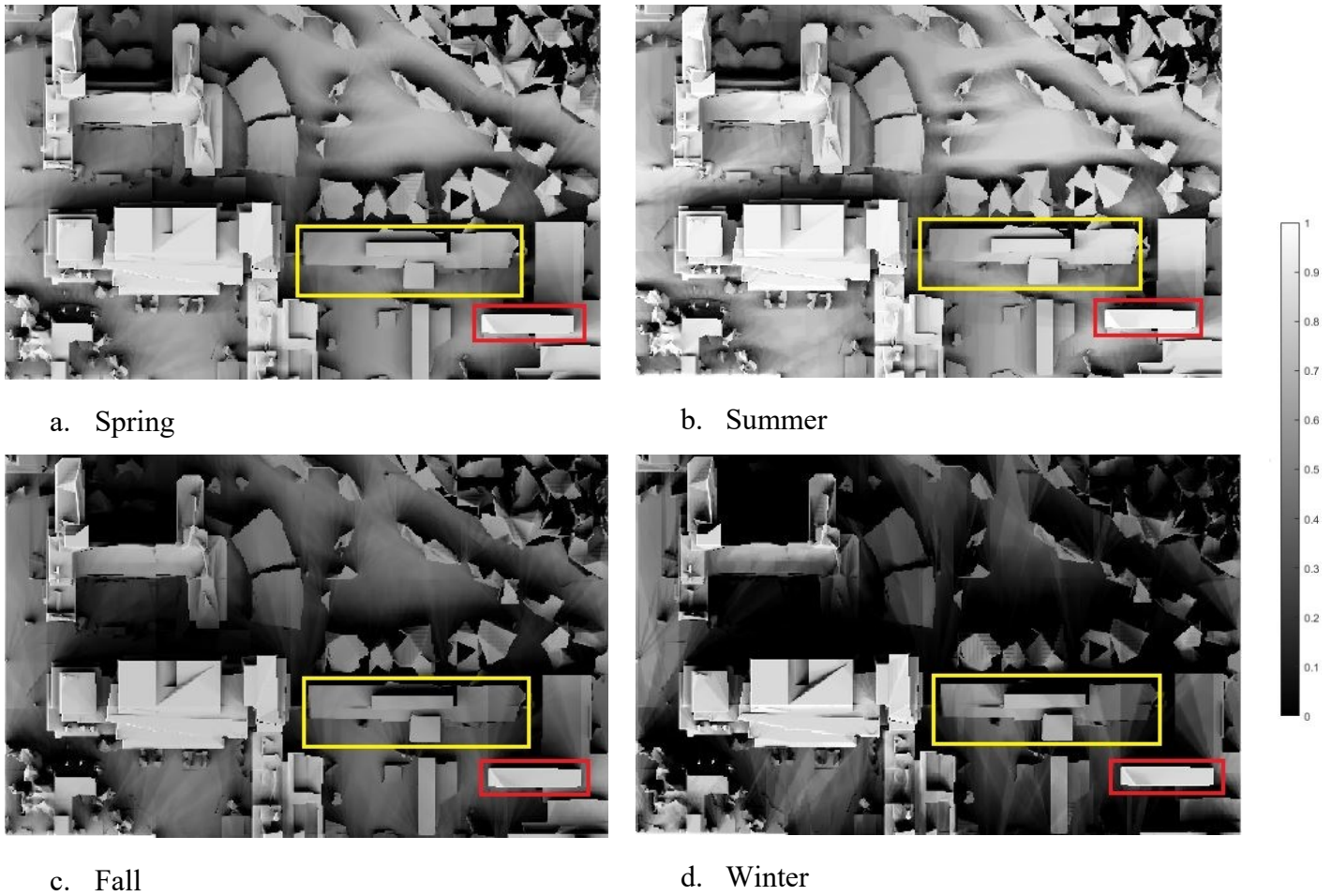
c. Fall      d. Winter

Figure 23. Shading map of the EAS building at a) spring, b) summer, c) fall, and d) winter

## 4.3    Validating Solar Radiation Model and Annual Electricity Generation

The clear-sky global horizontal radiation, the base for other calculations, is validated with the NASA Prediction of Worldwide Energy Resources [86]. The daily comparison of present study data and the mentioned reference is depicted in Figure 24. The difference between the current work and the data provided by NASA is 4.31%, which is acceptable.
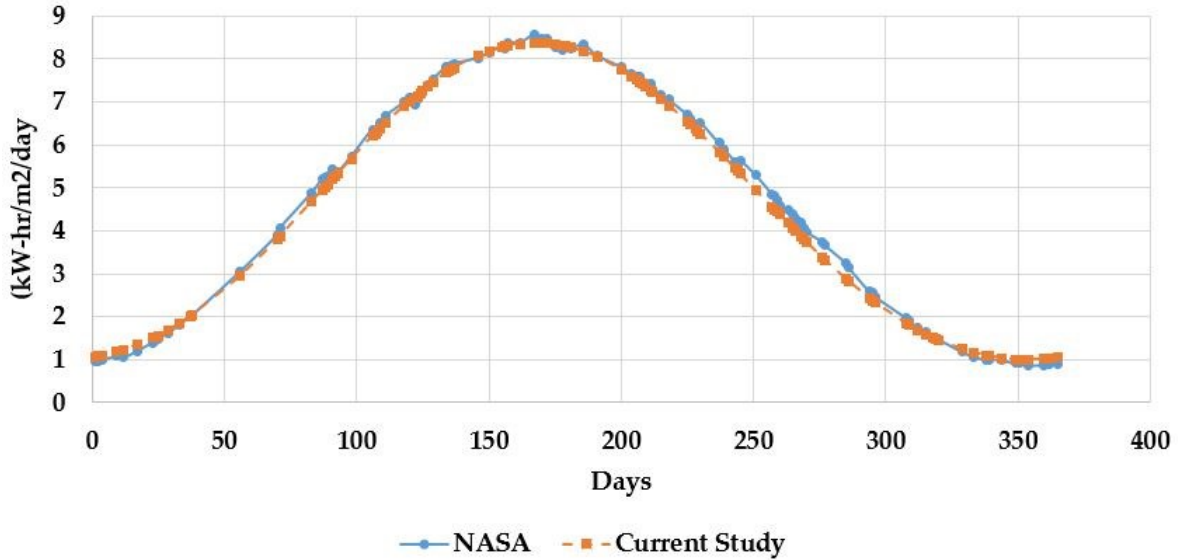
Figure 24. Daily clear-sky global horizontal radiation comparison of the current study and NASA

In the next step, Figure 25 compares the yearly electricity generation of the present work and PVWatts® at different tilt angles and a fixed azimuth angle (south-facing) of the PV system installed on the ADMIN building's roofs. Inter-row spacing is also set to one meter. Note that PVWatts® considers the mutual shading effect on PV arrays with one-axis tracking and does not consider that effect when fixed roof-mounted arrays are used [87].
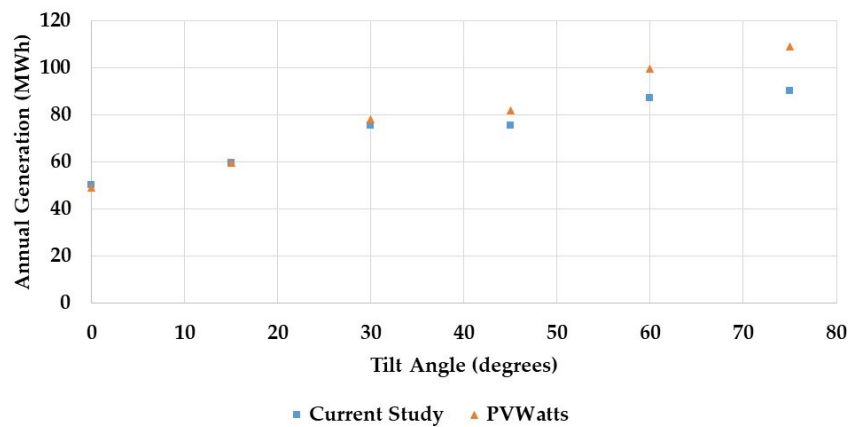


Figure 25. Comparing current work PV system yearly output and PVWatts® for the ADMIN building

52

According to Figure 25, for tilt angles greater than 45 degrees, a considerable difference is observed between the current study and PVWatts output (between 10 to 20%). The reason is that the PVWatts does not consider the mutual shading of PV arrays, so when the tilt angle increases at a fixed inter-row spacing, the shadow length created in the back arrays becomes more remarkable in the current study PV system output. On the other hand, the annual production difference between the proposed method and PVWatts$^{®}$ for the lower tilt angles is less than 5%.

The last two figures clearly validate the solar radiation model used in this study.

## 4.4  Optimization Results

As mentioned in the previous chapter, the space search method is used to find the optimum layout since the optimization problem is non-linear and defining an explicit formula between control variables is impossible due to the irregular shapes of the roofs. This section shows the results of the five attitudes of decision-makers about economic and environmental factors for the three buildings, which are elaborated on in the following subsections.

### 4.4.1  Administration Building (ADMIN)

The ADMIN building has two flat roofs, as presented in the previous sections. Table 3 represents the optimum values of control variables for the ADMIN building, considering the different attitudes of stakeholders.

Table 3 Optimum control variables values for various economic and environmental attitudes for the ADMIN building

| Multiplier $a$ (Economic) | Multiplier $b$ (Environmental) | Optimum $L_{ir}$ | Optimum $\beta$ | Optimum $\gamma$ |
|---|---|---|---|---|
| 1.00 | 0.00 | 3.5 m | 45° | 20° |
| 0.75 | 0.25 | 1.5 m | 50° | 20° |
| 0.50 | 0.50 | 1.0 m | 65° | 0° |
| 0.25 | 0.75 | 1.0 m | 85° | 15° |
| 0.00 | 1.00 | 1.0 m | 85° | 15° |

As shown in Table 3, as the economic vision decreases and the decision-makers environmental vision increases, the distance between the arrays decreases from 3.5 m to 1.0 m. The tilt angle also increases from 45° (a few degrees below location latitude) to 85° (almost vertical). The azimuth angle does not follow the same increasing or decreasing pattern as the other two variables, but it generally changes between south-facing and 20 degrees toward the west. Another observation could be the state when the economic and environmental visions are equal (50%) when the optimum azimuth angle is zero degrees. As will be shown in Figure 28, due to the non-linearity of the problem because of the shape of the roofs, the number of panels changes slightly and without a specific pattern by changing their azimuth angle around a particular one close to the optimum region in a fixed tilt angle and inter-row spacing, which leads to minor difference in payback time and $CO_2$ emission savings and ultimately $Ind_{eco-env}$. As a result, the optimal azimuth angle could change a range of values for different economic and environmental visions. The corresponding layouts of different attitudes for the ADMIN building are presented in Figure 26.

$a = 1.00, b = 0.00$

$a = 0.75, b = 0.25$

$a = 0.50, b = 0.50$

$a = 0.25, b = 0.75$

$a = 0.00, b = 1.00$
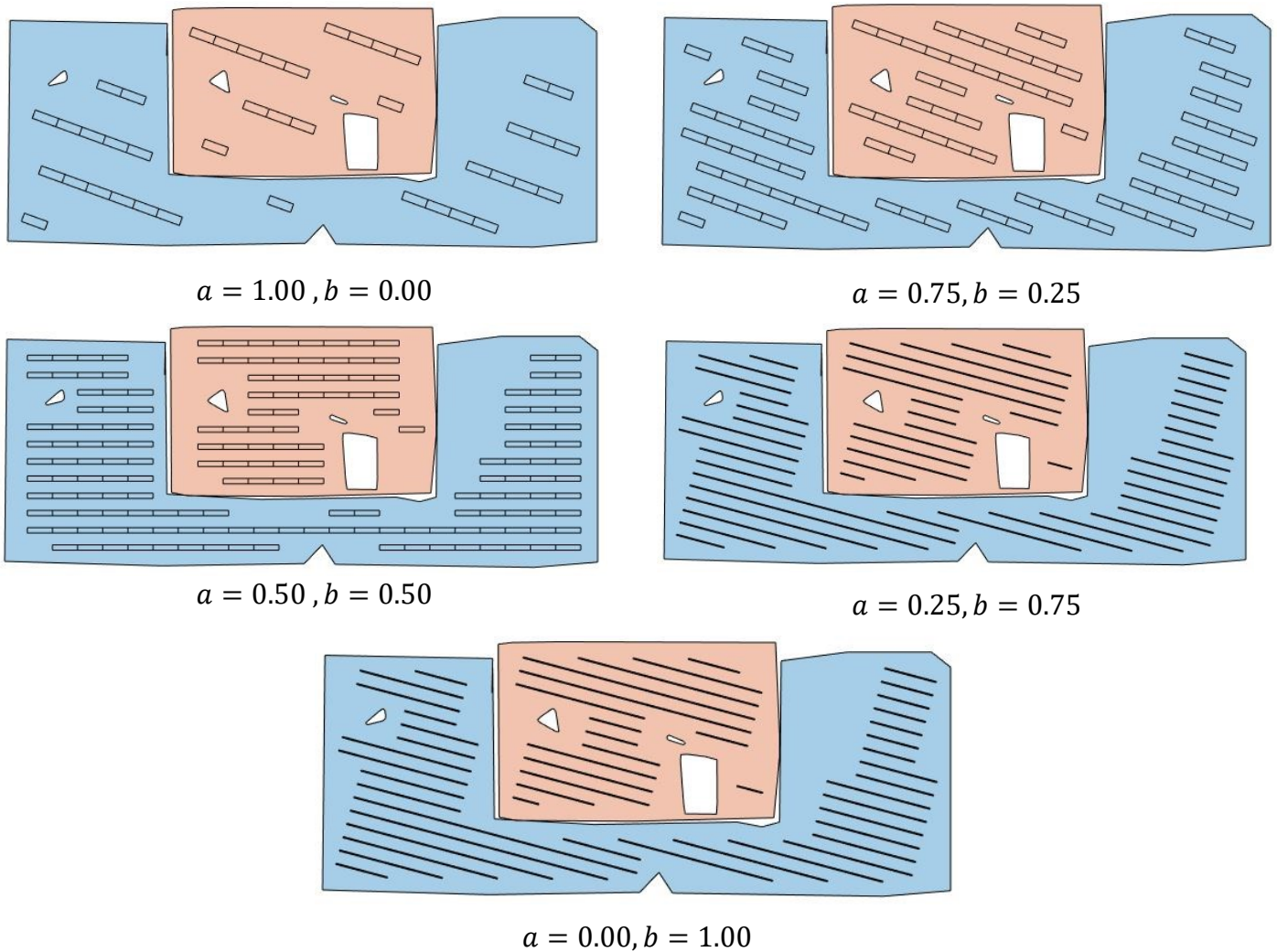
Figure 26. Optimum layouts of different economic and environmental attitudes for the ADMIN building

The impact of roofs shapes and existing obstacles on PV modules placement on roofs are considerable. Also, as can be obtained from Table 3 and Figure 26, changing the environmental attitude from 75 percent to fully environmental does not alter the optimum layout of the PV system. Note that the modules in Figure 26 are shown from the top-down view, which is why as the tilt angle of panels increases, they are seen as narrower. To better understand the impact of the decision makers' economic and ecological vision on the details of the installed PV systems, Table 4

represents the annual output, the number of PV modules, payback time, and $CO_2$ emission savings amount for various economic and environmental scenarios.

Table 4. ADMIN annual output, modules number, payback time, and $CO_2$ emission saving per year

| Multiplier $a$ (Economic) | Multiplier $b$ (Environmental) | Annual Output(MWh) | Number of PV Modules | Payback (years) | $CO_2$ Emission Saving (Tons/Year) |
|---|---|---|---|---|---|
| 1.00 | 0.00 | 20.75 | 42 | 22.40 | 20.21 |
| 0.75 | 0.25 | 44.42 | 95 | 23.67 | 43.17 |
| 0.50 | 0.50 | 65.32 | 172 | 29.15 | 62.91 |
| 0.25 | 0.75 | 68.72 | 209 | 33.69 | 65.70 |
| 0.00 | 1.00 | 68.72 | 209 | 33.69 | 65.70 |

One of the most significant results from the data in Table 4 is that a 25% increase in environmental attitude from nothing escalates annual production, carbon dioxide emission savings and the number of panels more than twice, while the payback time is increased by about one year. According to Table 3, this annual output doubling happens by reducing two meters inter-row spacing, increasing 5 degrees of tilt angles, and keeping the same azimuth angle. However, another 25 percent increase in the environmental perspective from 25 percent to 50 percent does not have the same effect as before. With an 80% increase in panels, the annual output and $CO_2$ emission savings increase by less than 50%, and the return on investment takes 5.5 more years. The reason could be investigated in inter-row spacing and PVs' tilt angles. For the second 25% increase in environmental attitude, regarding Table 3, the distance between the arrays decreases by another half a meter and their tilt angle increases by 15 degrees. Due to these changes in the layout, the mutual shading of PV arrays significantly reduces the production of the PV system so that an 80% increase in panels numbers will not have the same effect on increasing production. The arrays' shading impact is even more understandable in the subsequent 25% increase in environmental

56

views from 50% to 75%. At this stage, it is no longer possible to reduce the distance between the arrays due to constraints, and only the tilt angle of the PVs increases by 20 degrees. In this case, even though about 22% of panels have been added, only 5% is added to the yearly electricity generation. Finally, an increase of another 25% and reaching an entirely environmental perspective will not affect the layout of the PV system compared to the previous state, as it is impossible to reduce the distance between the arrays or increase their tilt angle due to constraints.

Another noteworthy point is the lack of panels in some arrays due to the shading of other objects, especially on the elevated roof. The higher elevation of the rooftop marked in orange compared to the roof marked in blue is the main reason for removing a few panels from the top right section of the blue roof, as demonstrated in Figure 27. Note that since the layout for entirely and 75% environmental attitude are the same, Figure 27 shows those two states once. Moreover, according to Table 5, shading impacts of existing obstacles, parapets on roofs, and roof elevation difference result in about a 28 percent reduction in annual electricity generation for all states of economic and environmental perspectives.

Table 5 Comparing the shading impact of objects on the PV system annual output for different economic and environmental attitudes in ADMIN building

| Multiplier $a$ (Economic) | Multiplier $b$ (Environmental) | Annual Output with Obstacles Shading (MWh) | Annual Output without Obstacles Shading (MWh) | Annual Output Difference (%) |
|---|---|---|---|---|
| 1.00 | 0.00 | 20.75 | 29.21 | 28.96 |
| 0.75 | 0.25 | 44.42 | 61.74 | 28.05 |
| 0.50 | 0.50 | 65.32 | 91.60 | 28.69 |
| 0.25 | 0.75 | 68.72 | 96.30 | 28.64 |
| 0.00 | 1.00 | 68.72 | 96.30 | 28.64 |

| With obstacles shading | Without obstacles shading |

$$a = 1.00 , b = 0.00$$

| With obstacles shading | Without obstacles shading |

$$a = 0.75, b = 0.25$$

| With obstacles shading | Without obstacles shading |

$$a = 0.50 , b = 0.50$$

| With obstacles shading | Without obstacles shading |

$$a = 0.25, b = 0.75 \ \& \ a = 0.00, b = 1.00$$
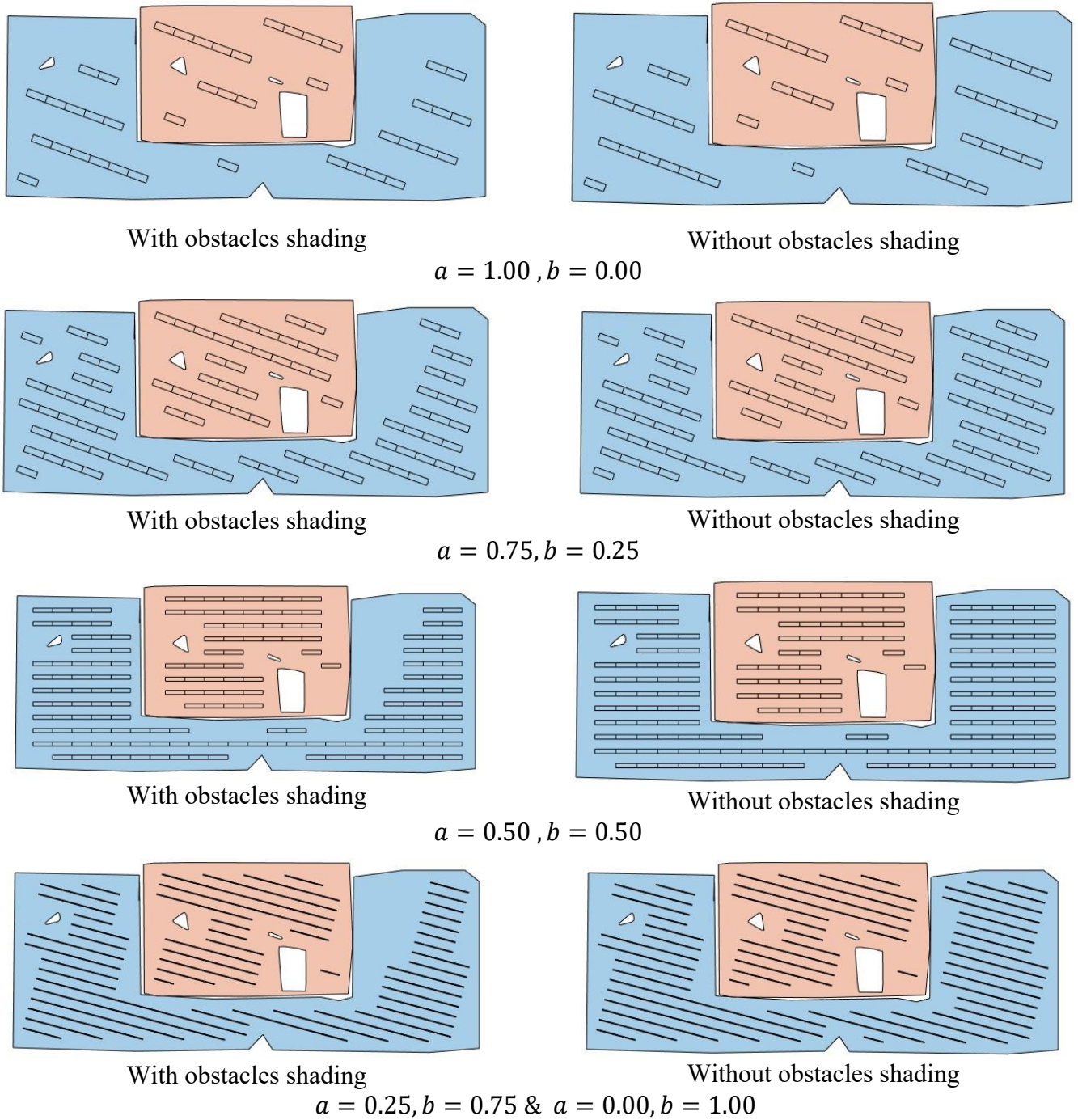
Figure 27. Comparison of the PV system layout in the ADMIN building with and without obstacles shading impact for different economic and environmental attitudes

Figure 28 shows the changes in the objective function with tilt and azimuth angles at optimal distances of arrays for each of the economic-environmental scenarios.
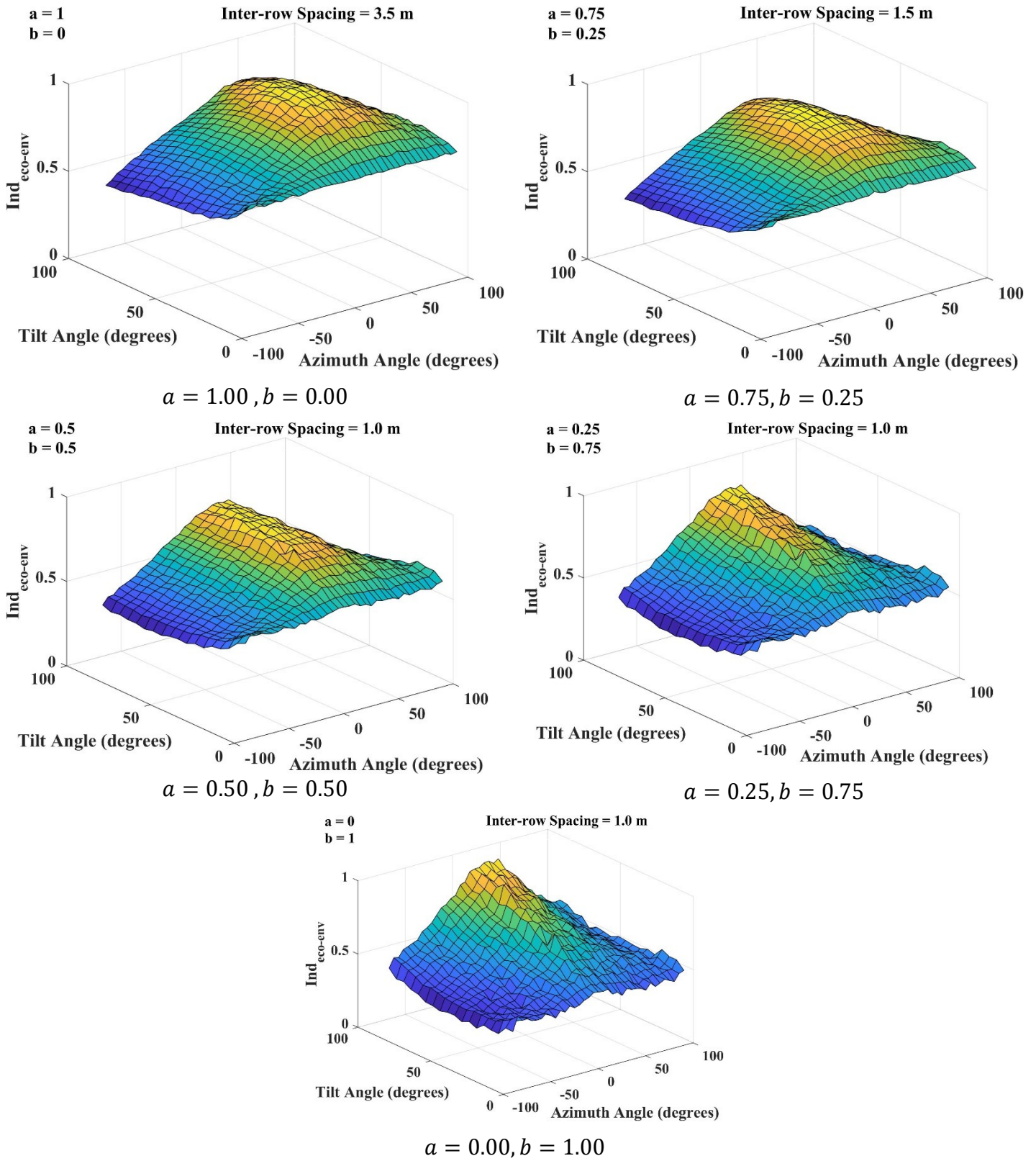
Figure 28. Variation of $Ind_{eco-env}$ with tilt and azimuth angle at the optimum inter-row spacing for different economic and environmental approaches in the ADMIN building

According to Figure 28, the optimal distances between arrays and tilt angles change drastically in different economic and environmental vision modes. Still, the azimuth angle varies between zero (due south) and 20 degrees to the west. In normal conditions, when panels are oriented toward the south and north in the northern and southern hemispheres, respectively, they could generate more electricity [67]. However, in the current study, the sky cloudiness, surrounding obstacles shading, and PV placement, the modules' azimuth angle deviate from the south toward the west in some economic and environmental attitudes. In addition, building electricity load distribution could be effective in modules' orientation; however, hourly loads are more significant than the hourly generation in the investigated building, so it could not affect PV panels' azimuth angles. Moreover, as mentioned before, by decreasing the economic perspective of the project stakeholders, the tilt angle moves from the mid-range towards higher angles.

### 4.4.2 Cameron Science, Engineering, Business Library Building (CAM)

As mentioned in the previous sub-sections, the CAM building has both types of flat and slanted roofs, 14 slanted roofs in the middle and one flat roof around them. The optimum layout for different economic and environmental perspectives is presented in Table 6. One should bear in mind that the control variables are applied only for the flat roof, and the tilt and azimuth angles of panels on slanted roofs are identical to the slanted roofs' slope and orientation.

Figure 29 also shows the PV system layout on the roofs of the CAM building with different economic and environmental attitudes.

Table 6. Optimum control variables values for various economic and environmental attitudes for the CAM building

| Multiplier $a$ (Economic) | Multiplier $b$ (Environmental) | Optimum $L_{ir}$ | Optimum $\beta$ | Optimum $\gamma$ |
|---|---|---|---|---|
| 1.00 | 0.00 | 3.0 m | 50° | 0° |
| 0.75 | 0.25 | 1.5 m | 45° | 0° |
| 0.50 | 0.50 | 1.0 m | 75° | 10° |
| 0.25 | 0.75 | 1.0 m | 85° | 20° |
| 0.00 | 1.00 | 1.0 m | 85° | 20° |
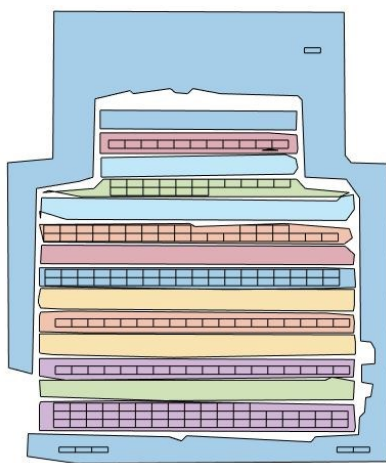


$a = 1.00 , b = 0.00$
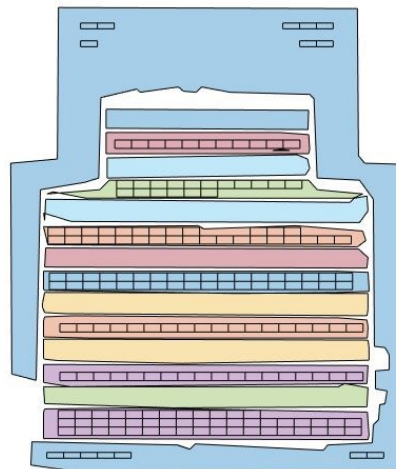
$a = 0.75, b = 0.25$
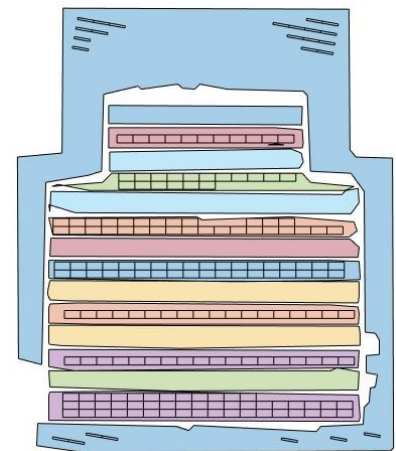
$a = 0.50 , b = 0.50$
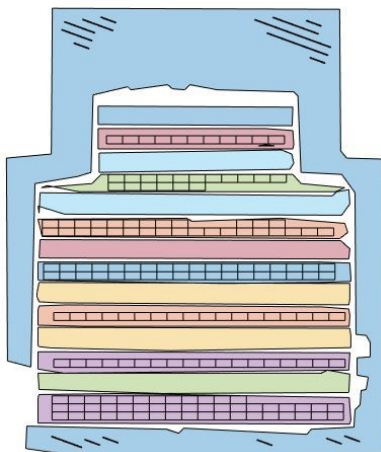
$a = 0.25, b = 0.75$
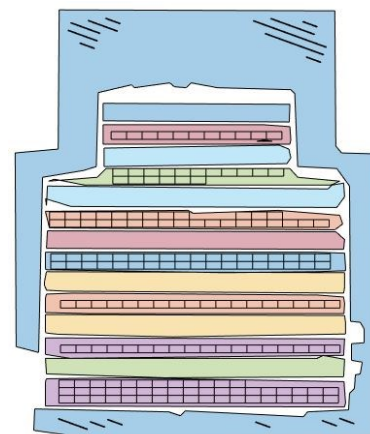
$a = 0.00, b = 1.00$

Figure 29. Optimum layouts of different economic and environmental attitudes for the CAM building

As shown in Figure 29, the slanted roofs play the primary role in electricity generation in the CAM building since most modules are installed on them. As a result, the PV system output is expected not to change significantly. It is also noteworthy that PV modules are not installed on sloped roofs facing north because they do not receive direct sunlight in the northern hemisphere. In addition, on a flat roof, it is not possible to install a panel in the thin parts of the left and right due to keeping a minimum distance from the roof edges. Another critical point is the lack of panel installation in major parts of the flat roof due to shading, which will be discussed later. Table 7 illustrates the annual electricity generation, the number of PV modules, payback time, and $CO_2$ emission savings amount from various economic and environmental perspectives.

As shown in Table 7, different attitudes do not change the annual output and $CO_2$ emission savings remarkably. This is mainly because of almost the same number of panels in different economic-environmental visions resulting from the dominance of slanted roofs over the only existing flat roof.

Table 7. CAM annual output, modules number, payback time, and $CO_2$ emission saving per year

| Multiplier $a$ (Economic) | Multiplier $b$ (Environmental) | Annual Output(MWh) | Number of PV Modules | Payback (years) | $CO_2$ Emission Saving (Tons/Year) |
|---|---|---|---|---|---|
| 1.00 | 0.00 | 75.09 | 184 | 27.12 | 72.56 |
| 0.75 | 0.25 | 78.43 | 193 | 27.24 | 75.78 |
| 0.50 | 0.50 | 80.89 | 203 | 27.78 | 78.09 |
| 0.25 | 0.75 | 81.43 | 207 | 28.14 | 78.56 |
| 0.00 | 1.00 | 81.43 | 207 | 28.14 | 78.56 |

Figure 30 demonstrates the shading impact of objects on PVs' installation, as mentioned earlier. The primary shading effect is due to the existing 14 elevated slanted roofs in the middle of the CAM ceiling compared to the flat roof. To better understand why many panels are removed from

the flat roof, we must refer to Figure 13 and Figure 22. Figure 13 vividly specifies that the midsection slanted roofs are higher than the surrounding flat roof. Furthermore, as can be seen from the shading maps of Figure 22, most of the flat roof of the CAM is behind those slanted high-elevated roofs, so that region is under shading most of the time. Therefore, most of this part is less than the defined brightness threshold for installing panels, and panels are not installed on those parts. Table 8 also reveals the objects' shading impact on annual output.



| With obstacles shading | Without obstacles shading |
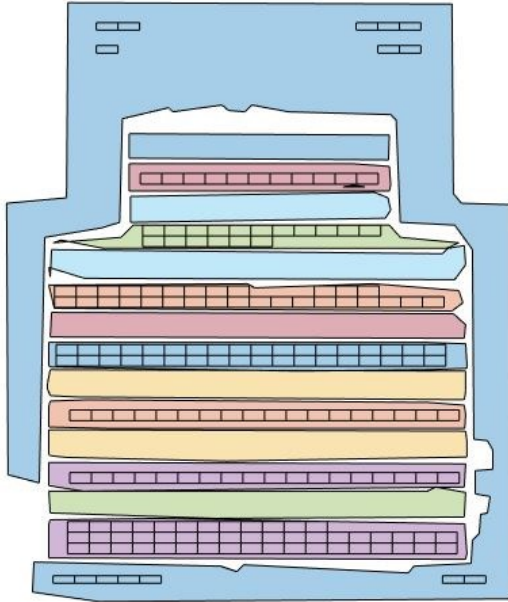
$$a = 1.00\,, b = 0.00$$

With obstacles shading        Without obstacles shading

$$a = 0.75, b = 0.25$$

With obstacles shading        Without obstacles shading
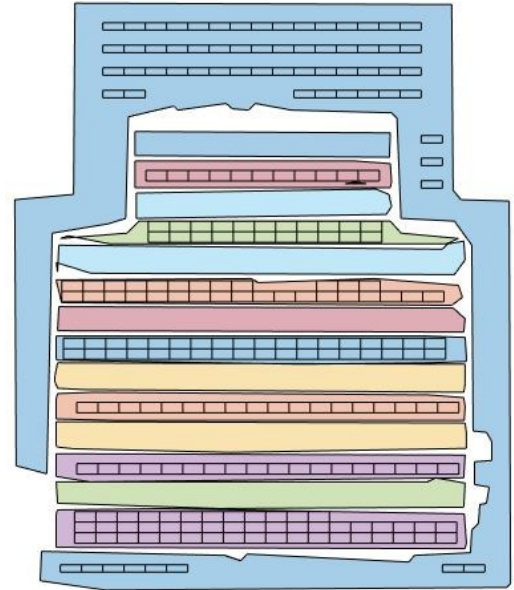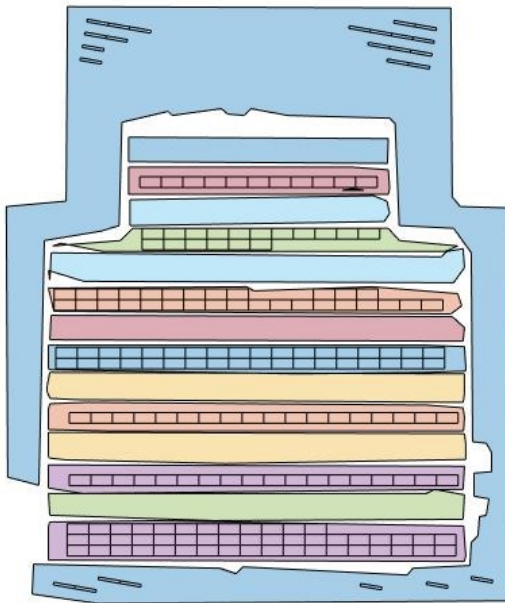
$$a = 0.50, b = 0.50$$

With obstacles shading          Without obstacles shading
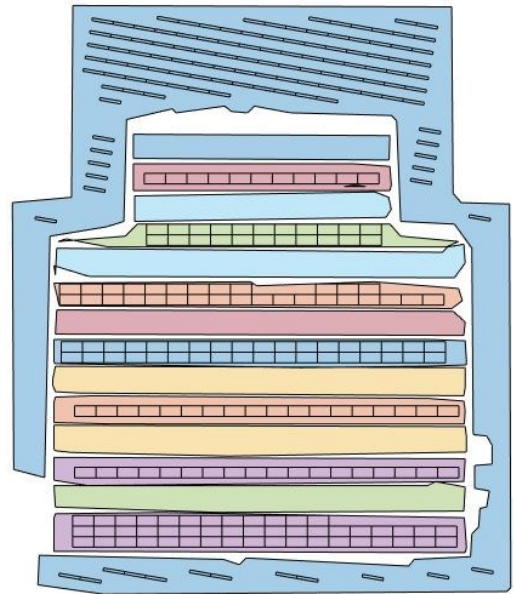
$$a = 0.25, b = 0.75 \ \& \ a = 0.00, b = 1.00$$
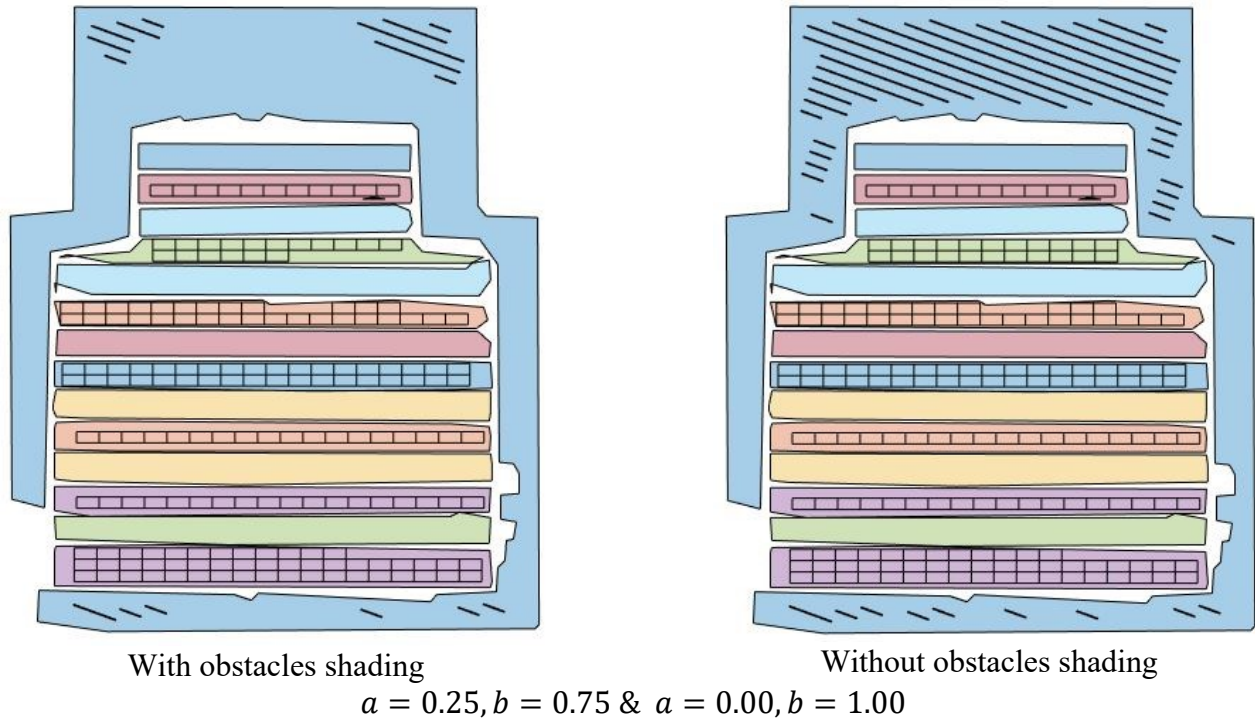
Figure 30. Comparison of the PV system layout in the CAM building with and without obstacles shading impact for different economic and environmental attitudes

Table 8. Comparing the shading impact of objects on the PV system annual output for different economic and environmental attitudes in CAM building

| Multiplier $a$ (Economic) | Multiplier $b$ (Environmental) | Annual Output with Obstacles Shading (MWh) | Annual Output without Obstacles Shading (MWh) | Annual Output Difference (%) |
|---|---|---|---|---|
| 1.00 | 0.00 | 75.09 | 121.13 | 38.01 |
| 0.75 | 0.25 | 78.43 | 131.20 | 40.22 |
| 0.50 | 0.50 | 80.89 | 153.43 | 47.28 |
| 0.25 | 0.75 | 81.43 | 153.35 | 46.90 |
| 0.00 | 1.00 | 81.43 | 153.35 | 46.90 |

Note that when the shadow effect is taken into account, due to the removal of many panels from the flat roof, the annual production values are much closer to each other than when the shadow effect is not considered. In addition, neglecting the shading impacts of objects causes the yearly electricity production to be over predicted between 38% and 47% regarding which economic and environmental attitude is applied.

Finally, Figure 31 demonstrates the changes in the objective function with tilt and azimuth angles at optimal distances of PV arrays for each of the economic-environmental perspectives. The most noticeable result from the graphs in Figure 31 is that they are almost flat, meaning that the objective function is nearly insensitive to control variables. Changing the control variables only affects the number and arrangement of panels on the flat roof. In addition, as mentioned many times, the adverse shading impacts of the middle slanted roofs result in not installing enough panels on the flat roof. Thus, there is a minimal possibility of changing the number of panels and annual output, resulting in the almost constant value for the objective function. Also, as shown in the graphs, reducing the distance between the arrays causes the graphs to change slightly from the smooth behaviour because there is a possibility of increasing the number of panels. This non-smoothness is evident around the optimal tilt and azimuth angles and when inter-row spacing is one-meter.

$a = 1.00 , b = 0.00$

$a = 0.75 , b = 0.25$

$a = 0.50 , b = 0.50$

$a = 0.25 , b = 0.75$

$a = 0.00 , b = 1.00$
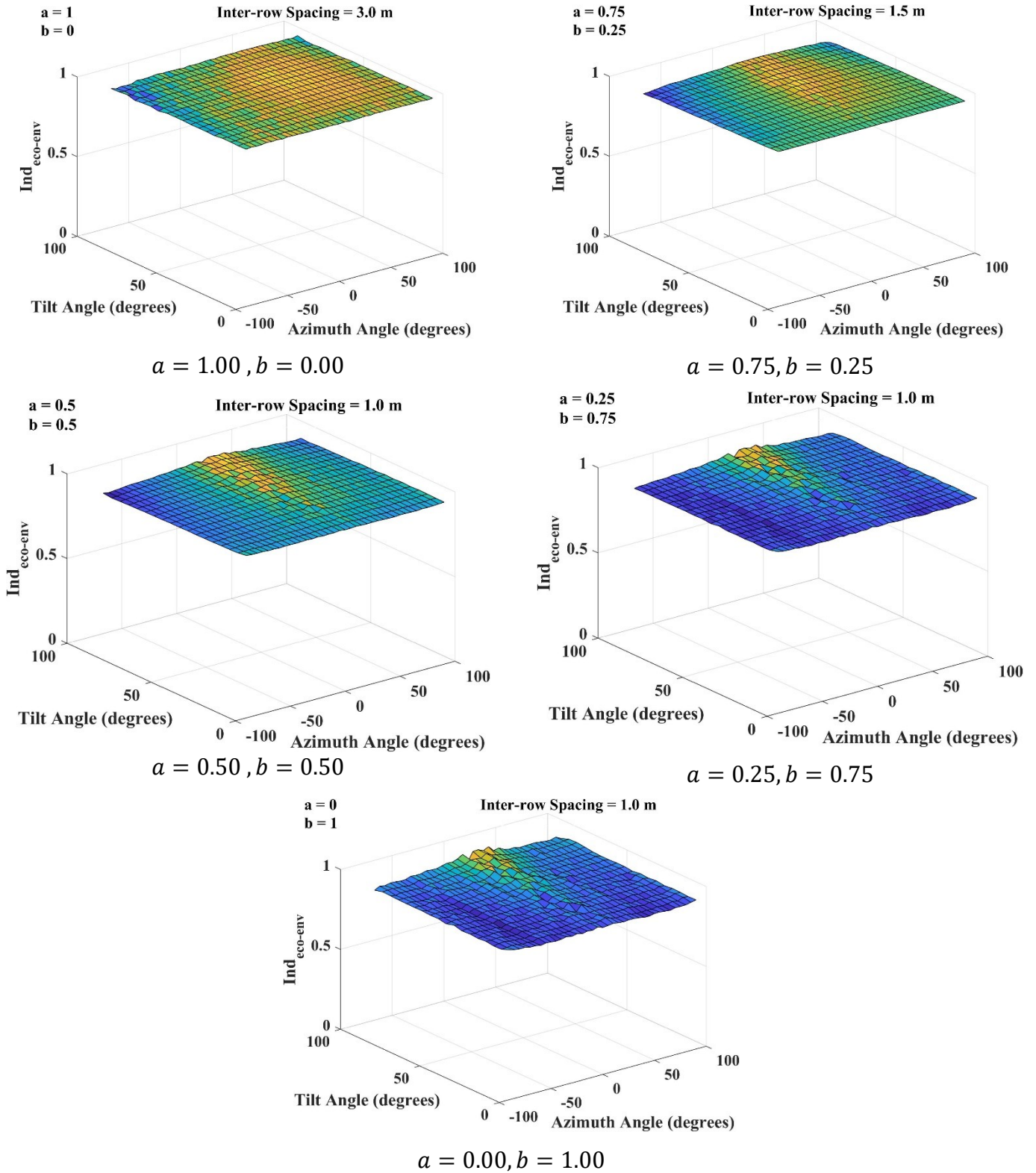
Figure 31. Variation of $Ind_{eco-env}$ with tilt and azimuth angle at the optimum inter-row spacing for different economic and environmental approaches in the CAM building

### 4.4.3　Earth and Atmospheric Sciences Building (EAS)

As shown in Figure 14, the EAS building has only flat roofs, with a quite large high elevated top in the middle of the building and many small obstacles on different parts of the roofs. Table 9 provides the optimum values of inter-row spacing, tilt and azimuth angles for the EAS building considering decision-makers different economic and environmental perspectives.

Table 9. Optimum control variables values for various economic and environmental attitudes for the EAS building

| Multiplier $a$ (Economic) | Multiplier $b$ (Environmental) | Optimum $L_{ir}$ | Optimum $\beta$ | Optimum $\gamma$ |
|---|---|---|---|---|
| 1.00 | 0.00 | 4.5 m | 50° | 15° |
| 0.75 | 0.25 | 1.5 m | 45° | 15° |
| 0.50 | 0.50 | 1.0 m | 70° | 10° |
| 0.25 | 0.75 | 1.0 m | 85° | 15° |
| 0.00 | 1.00 | 1.0 m | 85° | 15° |

The distance between the arrays when the project stakeholder attitude is completely economical is the maximum possible value, 4.5 m. The amount is reduced significantly by three meters with a 25% reduction in economic viewpoint. Decreased economic attitude eventually leads to the minimum distance between arrays which is 1.0 m. When the environmental perspective is low (none or 25 percent), the tilt angle of the panels is slightly less than the latitude angle of the installation site, and it moves towards higher tilt angles as the environmental attitude increases. For the azimuth angle, except for the case where the economic and environmental vision is equal, panels should be installed at an angle of 15 degrees to the west. Accordingly, Figure 32 shows the optimal layout of PV systems from various economic and environmental perspectives.
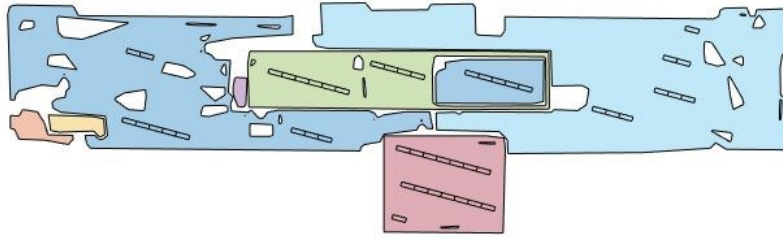
$$a = 1.00, b = 0.00$$
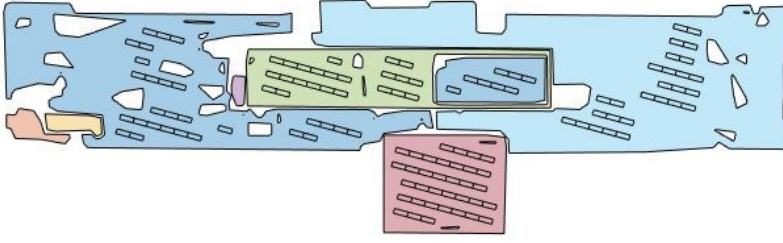


$$a = 0.75, b = 0.25$$
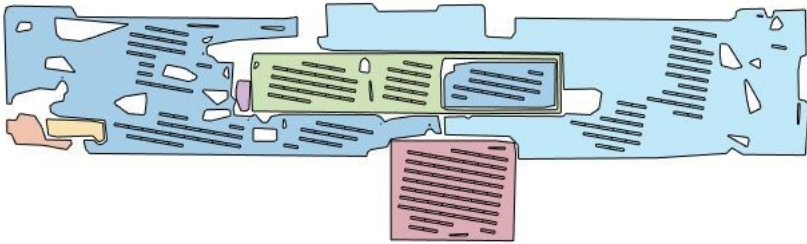


$$a = 0.50, b = 0.50$$
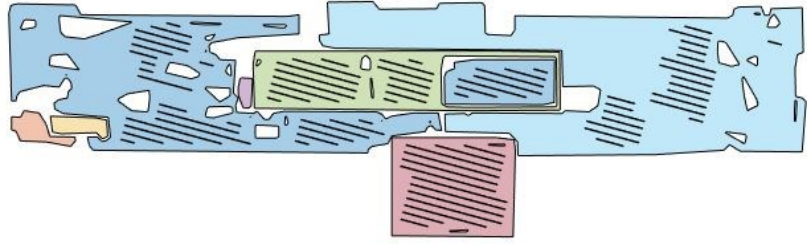


$$a = 0.25, b = 0.75$$
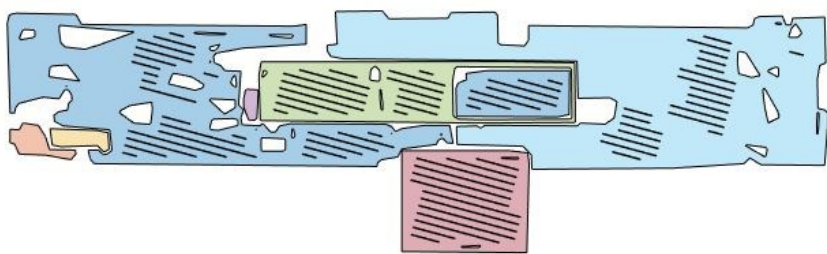


$$a = 0.00, b = 1.00$$

Figure 32. Optimum layouts of different economic and environmental attitudes for the EAS building

In the EAS building, as seen in Figure 32, the critical factors in specifying modules arrangement are the presence of obstacles and irregular shapes of roofs. However, the objects' shading impact is also considerable and will be discussed in the following. The corresponding annual output, number of the PV modules, payback time and $CO_2$ emission saving for each of those above-mentioned optimum layouts are illustrated in Table 10.

Table 10. EAS annual output, modules number, payback time, and $CO_2$ emission saving per year

| Multiplier $a$ (Economic) | Multiplier $b$ (Environmental) | Annual Output(MWh) | Number of PV Modules | Payback (years) | $CO_2$ Emission Saving (Tons/Year) |
|---|---|---|---|---|---|
| 1.00 | 0.00 | 20.86 | 49 | 26.00 | 20.19 |
| 0.75 | 0.25 | 48.99 | 121 | 27.34 | 47.32 |
| 0.50 | 0.50 | 71.73 | 215 | 33.20 | 68.62 |
| 0.25 | 0.75 | 80.93 | 283 | 38.76 | 76.70 |
| 0.00 | 1.00 | 80.93 | 283 | 38.76 | 76.70 |

Based on Table 10 data, annual electricity production and $CO_2$ emission saving will almost quadruple by shifting from the economic to the environmental perspective. At the same time, the return on investment will take 12 more years. Notably, according to Table 10, by reducing the economic attitude from 100% to 75%, the number of panels, annual production and $CO_2$ emission saving can be more than doubled, while the payback time has been increased by almost a year. However, reducing the economic outlook from 75% to below will no longer have the same effect.

Next, object shadings' impact is investigated on the allocation of PV panels on EAS roofs. Figure 33 compares the results of PV systems arrangement with and without considering the objects' shading impact. Note that 100% and 75% environmental visions do not change the arrangement of the PV panels.

With obstacles shading       Without obstacles shading

$$a = 1.00, b = 0.00$$

With obstacles shading       Without obstacles shading

$$a = 0.75, b = 0.25$$

With obstacles shading       Without obstacles shading

$$a = 0.50, b = 0.50$$

With obstacles shading       Without obstacles shading

$$a = 0.25, b = 0.75 \ \& \ a = 0.00, b = 1.00$$
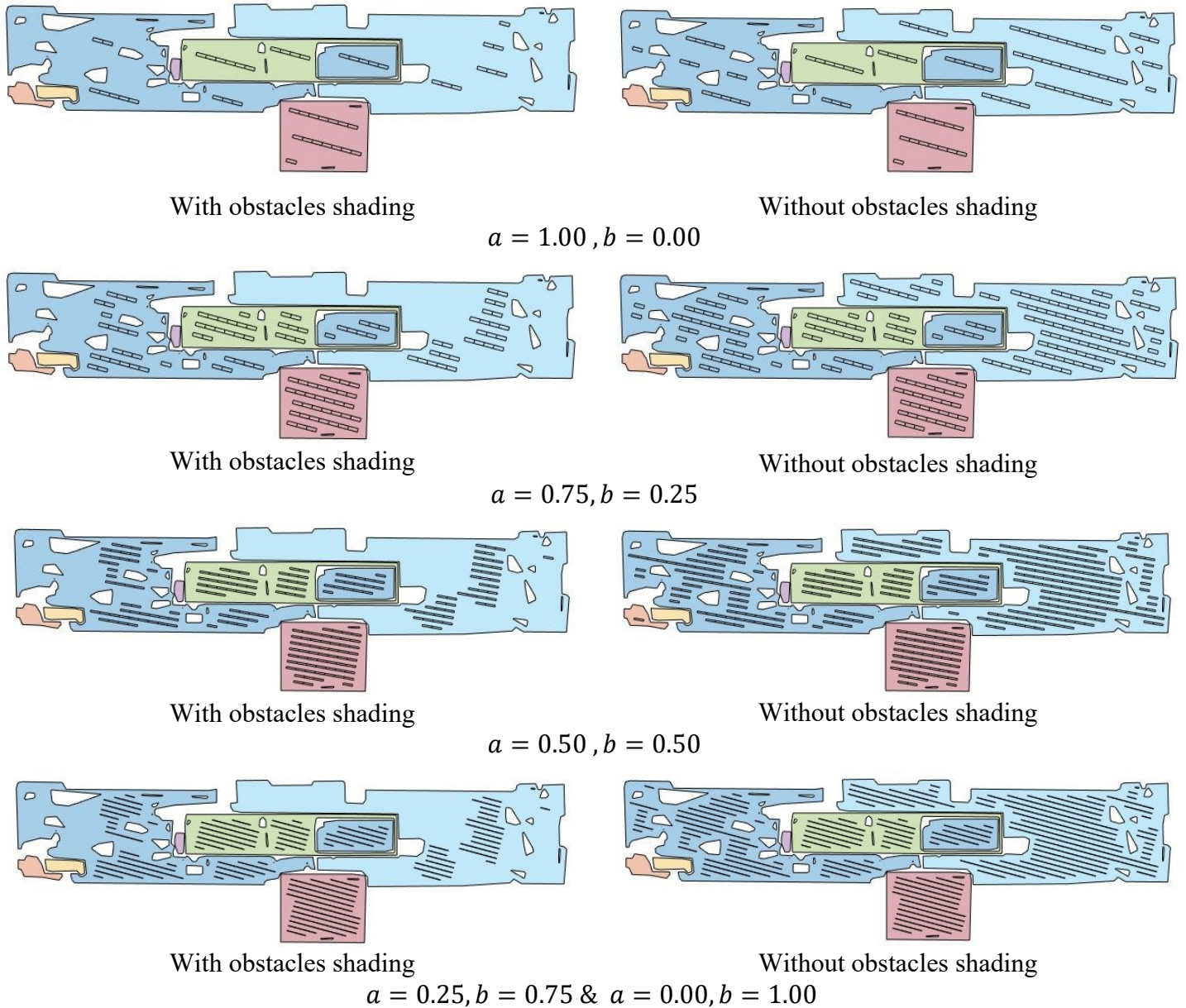
Figure 33. Comparison of the PV system layout in the EAS building with and without obstacles shading impact for different economic and environmental attitudes

The impact of objects' shading is eye-catching in Figure 33, as more than half of the modules are removed from the PV system. In the EAS building, high-elevated roofs in the building itself and the tall building neighbouring of the EAS have effects on dismissing panels. For instance, the panels that could have been on the top and top right behind the two higher roofs have been removed due to those two roofs (green and dark blue roofs in center) shadow casting. On the other hand,

the panels that have been removed in the lower right part of the EAS roofs are mainly due to the presence of a tall building in the southeastern part of the EAS. The shading of other obstacles on roofs is also effective in not installing panels in some regions.

Table 11 also shows the objects' shading impact on annual electricity generation. About 62% of annual electricity generation is lost in the EAS building for various economic and environmental attitudes. This demonstrates how not considering the shading of objects in the analysis of photovoltaic systems can lead to unrealistic results.

Table 11. Comparing the shading impact of objects on the PV system annual output for different economic and environmental attitudes in EAS building

| Multiplier $a$ (Economic) | Multiplier $b$ (Environmental) | Annual Output with Obstacles Shading (MWh) | Annual Output without Obstacles Shading (MWh) | Annual Output Difference (%) |
|---|---|---|---|---|
| 1.00 | 0.00 | 20.86 | 58.45 | 64.31 |
| 0.75 | 0.25 | 48.99 | 125.99 | 61.12 |
| 0.50 | 0.50 | 71.73 | 189.69 | 62.19 |
| 0.25 | 0.75 | 80.93 | 212.75 | 61.96 |
| 0.00 | 1.00 | 80.93 | 212.75 | 61.96 |

Finally, like the other buildings, the variation in the objective function with tilt and azimuth angles at optimal inter-row spacing for each economic and environmental attitude is shown in Figure 34.

$a = 1.00 , b = 0.00$

$a = 0.75, b = 0.25$

$a = 0.50 , b = 0.50$

$a = 0.25, b = 0.75$

$a = 0.00, b = 1.00$
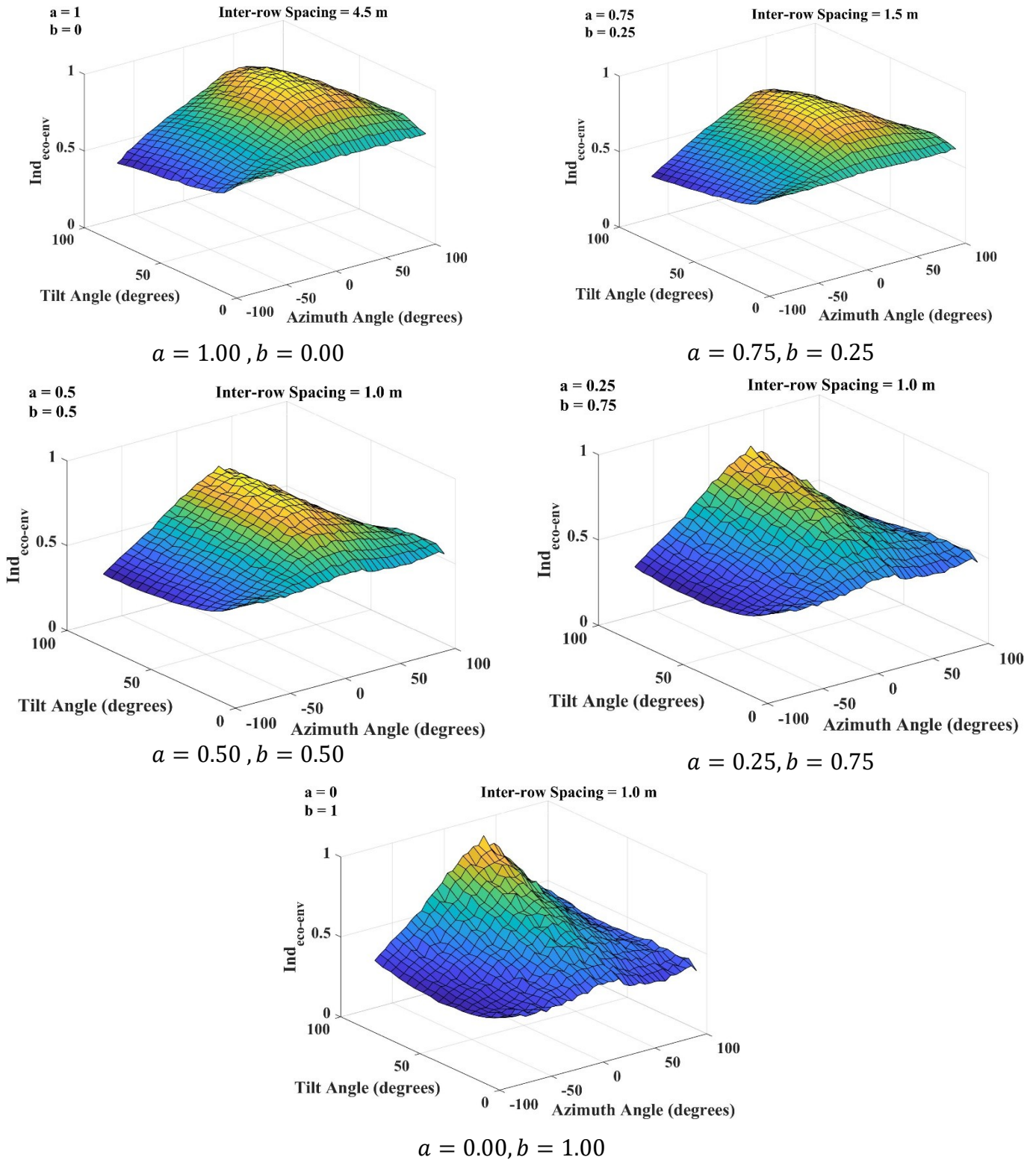
Figure 34. Variation of $Ind_{eco-env}$ with tilt and azimuth angle at the optimum inter-row spacing for different economic and environmental approaches in the EAS building

73

Overall, the behaviour of the graphs is similar to that of the ADMIN building, mainly due to the existence of only flat roofs in the ADMIN and EAS. As the economic viewpoint is reduced, the optimum tilt angle moves from mid-range toward higher tilt angles. However, in almost all attitudes, the azimuth angle remains constant at about 15 degrees to the west. Another point is that when the economic vision dominancy is equal to or greater than the environmental one, the orientation of panels to the west has better results than the same amount of rotation to the east, which the reason was stated earlier in the explanation of the graphs of the ADMIN building. Another point is that the maximum value of the objective function is one and occurs when the vision to implement the solar project is either entirely economic or environmental. While the maximum values of the objective function for 75%, 50%, and 25% economic viewpoint are 0.87, 0.84, and 0.92, respectively.

### 4.4.4 Sensitivity of Payback Results to Incentives

As mentioned in the previous sections, in the most economic vision, the payback times for the ADMIN, CAM, and EAS buildings are 22.40, 27.12, and 26.00 years, respectively, which means investing in solar projects from an economic perspective may not be feasible.

However, PV modules cost has been fallen dramatically in the last decades; still, the installation price of PV panels overshadows the benefit that could be obtained by saving electricity bills and selling surplus generated power to the grid. The other reason is the lower price of electricity in Alberta, Canada.

Other works have recently reported the non-feasibility of PV projects in some locations. For instance, Korsavi et al. [35] mentioned a more than 40 years payback time for Iran's electricity

price conditions. Christiaanse et al. [37] also reported that a 50% reduction in cost is needed to make feasible the PV project in Vancouver, British Colombia, Canada.

Incentives supplied by governments could help reduce the payback period significantly. For example, an incentive plan that existed for the residential and commercial solar program in Alberta, cancelled in 2019, provided $0.75 per installed watt [88,89]. The mentioned incentive is applied to see how much the payback time could be decreased for three buildings when the project owner's attitude is considered entirely economical, as represented in Table 12.

Table 12. Payback time with and without incentives for the entirely economic vision for three buildings

| Building | Payback Time without Incentives (Years) | Payback Time with Incentives (Years) |
|----------|----------------------------------------|--------------------------------------|
| ADMIN | 22.40 | 16.39 |
| CAM | 27.12 | 19.84 |
| EAS | 26.00 | 19.02 |

The results in Table 12 reveal that applying the cancelled incentive could reduce about 27 percent of the payback time of the photovoltaic projects. Although they may not be very economically satisfactory again, however, a return on investment occurs over the life of the panels for three buildings.

## 4.5    Discussion and Recommendations

The first point is the importance of roofs extraction with their complexities and details, such as unusual shapes and obstacles. As the results showed, these details can determine the optimal distances of arrays, tilt and azimuth angles. If the shapes are simplified and the roof details are removed, they lead to a general and rough solution for all buildings of the same region, as reported by previous studies and mentioned in the "Literature Review" chapter.

Considering the annual production outputs, $CO_2$ emission savings, and payback time of ADMIN and EAS buildings, one significant result is that changing the environmental vision from zero to 25% leads to a substantial increase in annual production and $CO_2$ emission savings while it is no significant change of the payback time. Of course, this is not the case in the CAM building because the shading of slanted roofs on the only flat rooftop prevents the installation of panels. In general, it is necessary to inform the stakeholders of commercial and educational buildings who want to implement a solar project on their facilities' roofs so that they do not look at the project only from an economic point of view. If the initial budget for the project is not the case, they can double the initial investment and get the same payback time while doubling $CO_2$ emission savings.

Contrary to what was mentioned in the previous paragraph, in all three buildings, the change in environmental vision from 100% to 75%, which is equivalent to a 25% economic vision change from none to 25%, does not change panels layout and consequently the annual production, $CO_2$ emission savings and payback time.

The next important issue is the impact of objects shading on PV systems' annual output. As the results show, between 28% and 65% of the annual production can be overshadowed by shading in three buildings. The first and most crucial factor in objects' shading impact around the panels is the difference in height between the roofs of a building. The next influential factor is a high building around the building under study. Finally, large obstacles on the roofs, parapets, and tall trees around investigated buildings also affect the yearly generation. This underscores the necessity of considering objects' shading impacts around PV systems, which has been almost neglected in previous studies. Another point in this regard is informing the project owners and design teams from the beginning to design roofs in a way to prevent shading as much as possible.

76

For all buildings, regardless of the economic and environmental point of view, the panels' orientation can be changed between south and twenty degrees to the west to achieve the panels' optimal arrangement. However, this is different for the tilt angle; if the economic perspective is superior to the environment, installing the panels with a slight angle (5 degrees) less than the region's latitude is better. With the predominance of the environmental perspective, panels' tilt angle will be tended to be vertical.

Also, the optimal distances between the arrays are large (3 to 4.5 meters) when the view is entirely economic. Still, as soon as the economic outlook is reduced by 25%, it is drastically reduced for all buildings and reaches 1.5 meters. Finally, for a 50 percent to non-economic view, the distance between the arrays for all three buildings is fixed at one meter.

The next point is the significance of providing incentives by the government. In the current economic conditions, installing solar panels on the roofs has a payback period of about 20 years, which can be discouraging and unacceptable for investors.

Last but not least, the values of $CO_2$ emissions savings provided in the results are primarily based on coal-fired power plants' $CO_2$ emission per kWh electricity generation. One could be interested in evaluating natural gas-fired power plants instead of coal-based ones. By comparing emissions of coal-fired and natural gas-fired, which are 1.01 kg and 0.41 kg of carbon dioxide equivalent per one kilowatt-hour [80], respectively, one could estimate the $CO_2$ emissions savings in natural gas stations are 60 percent less than the coal-based power plants.

# CHAPTER FIVE. CONCLUSIONS

One of the most neglected issues in installing rooftop photovoltaic systems is the significance of the project stakeholders' vision for installing PV modules. Apart from that, automation of finding the optimum arrangement of PV systems on roofs by considering their unusual shapes and turning project owners' vision into practice are other challenges in the field of roof-installed PV systems.

In this thesis, a search space optimization algorithm was developed to simultaneously implement stakeholders' economic and environmental attitudes in the arrangement of roof-installed PV modules. Different combinations of economic and environmental perspectives were examined in the range of entirely economic to the entire environmental view. Payback time (PBT) and $CO_2$ emission savings were considered economic and environmental criteria, respectively. Rooftops details such as shapes, existing objects, slopes, orientations, etc., were extracted from an automated roof recognition tool aided by computer vision. Furthermore, mutual shading impacts of PV arrays and shading effects of objects around PV panels like chimneys, parapets, trees, elevated roofs, and tall buildings were considered in the annual output and arrangement of panels. The framework was applied to three buildings located on the North Campus of the University of Alberta in Edmonton, Alberta, Canada.

The results revealed that having the least environmental vision (25%) compared to an entirely economic vision, more than double the number of panel installations and more than double the annual electricity generation and $CO_2$ emission savings, with the payback time increasing only by about one year. In general, as the environmental vision of stakeholders increases, the distance between the arrays decreases, and the tilt angle moves from angles slightly less than the latitude of the investigated location (53°) to the nearly right angle (85°); on the other hand, panels' azimuth

angle changes in any case between the direction of south and twenty degrees to the west. Another critical point is the undeniable importance of the objects' shading impact around the panels on their annual production, without which the yearly production results will be significantly overestimated. Finally, the results showed that such solar PV applications may not be economically viable for places with low electricity prices, especially if no incentives are present to support the application financially. As a result, roof-installed PV projects could be cost-effective if incentives are applied, and the cost of electricity increases in the future.

In terms of the thesis contribution, it can provide a better view and idea to other researchers working in roof-installed PV systems to be aware of roofs' complex shapes and details effects on PV modules arrangement and consider project stakeholders' economic and environmental visions in their analysis. The proposed model also could be used in any location if the sky clearness index, electricity prices and incentives are available. Furthermore, the developed tool could benefit municipalities and owners of commercial and educational buildings and any buildings with flat roofs.

One of the limitations of the current work is that the computation may be time-consuming if a fine discretized interval of control variables is needed. However, this could be overcome by increasing the computational power. Also, the model should be improved to consider smaller objects on roofs, such as small pipes. Furthermore, the brightness threshold was set to sixty percent for the current study but increasing or decreasing this threshold is expected to change annual output, payback time, and $CO_2$ emission savings. Moreover, the final brightness score used to estimate PV system output is averaged equally in operating hours. It would be better to find a timely weighted average or obtain the hourly brightness score if computation cost allows. It should also be noted that the

electricity consumption data from the building (at least on an hourly basis) is needed for the analysis. If such data is not available, available data from similar buildings can be used to create the needed data for the analysis. Finally, the clearness index data used in this thesis is based on one-year data due to a lack of data, and it is recommended that the average of several years should be considered for a more detailed analysis. The following could be recommended for future work:

- Investigating other optimization algorithms to reduce simulation time and consider complex shapes of roofs and objects on them.

- Studying the effect of brightness threshold for removing modules from the PV system in more detail since it could be variable for any location and any project owner's vision.

- Applying the procedure presented in this thesis to buildings facades to evaluate the entire solar potential of buildings skins.

- Investigating the possibility of installing panels with tilt angle on slanted roofs, especially with slopes close to the horizontal and its effect on annual production, $CO_2$ emission savings, and payback time

- Considering demand-side management using battery storage

- Considering the social aspects of adding PV systems into buildings skins alongside the economic and environmental aspects to cover the three pillars of sustainability.

# References

1.  Kannan, N.; Vakeesan, D. Solar energy for future world:-A review. *Renew. Sustain. Energy Rev.* **2016**, *62*, 1092–1105.

2.  IEA IEA, Evolution of solar PV module cost by data source, 1970-2020, IEA, Paris Available online: https://www.iea.org/data-and-statistics/charts/evolution-of-solar-pv-module-cost-by-data-source-1970-2020 (accessed on Oct 27, 2021).

3.  Yu, H.J.J.; Geoffron, P. Solar PV market and policies. In *Photovoltaic Solar Energy Conversion*; Elsevier, 2020; pp. 413–437.

4.  IEA IEA, Solar PV power generation in the Sustainable Development Scenario, 2000-2030, IEA, Paris Available online: https://www.iea.org/data-and-statistics/charts/solar-pv-power-generation-in-the-sustainable-development-scenario-2000-2030 (accessed on Oct 27, 2021).

5.  Cao, X.; Dai, X.; Liu, J. Building energy-consumption status worldwide and the state-of-the-art technologies for zero-energy buildings during the past decade. *Energy Build.* **2016**, *128*, 198–213.

6.  Langevin, J.; Harris, C.B.; Reyna, J.L. Assessing the potential to reduce US building CO2 emissions 80% by 2050. *Joule* **2019**, *3*, 2403–2424.

7.  Statista • Rooftop share in solar PV deployment 2022 | Statista Available online: https://www.statista.com/statistics/1172031/rooftop-share-in-solar-pv-deployment/ (accessed on Oct 27, 2021).

8. Cities and Pollution | United Nations Available online: https://www.un.org/en/climatechange/climate-solutions/cities-pollution (accessed on Feb 15, 2022).

9. Caird, S.; Roy, R.; Herring, H. Improving the energy performance of UK households: Results from surveys of consumer adoption and use of low-and zero-carbon technologies. *Energy Effic.* **2008**, *1*, 149–166.

10. EL-Kassaby, M.M. Monthly and daily optimum tilt angle for south facing solar collectors; theoretical model, experimental and empirical correlations. *Sol. Wind Technol.* **1988**, *5*, 589–596.

11. Siraki, A.G.; Pillay, P. Study of optimum tilt angles for solar panels in different latitudes for urban applications. *Sol. energy* **2012**, *86*, 1920–1928.

12. Kaddoura, T.O.; Ramli, M.A.M.; Al-Turki, Y.A. On the estimation of the optimum tilt angle of PV panel in Saudi Arabia. *Renew. Sustain. Energy Rev.* **2016**, *65*, 626–634.

13. Jacobson, M.Z.; Jadhav, V. World estimates of PV optimal tilt angles and ratios of sunlight incident upon tilted and tracked PV panels relative to horizontal panels. *Sol. Energy* **2018**, *169*, 55–66, doi:https://doi.org/10.1016/j.solener.2018.04.030.

14. Dhimish, M.; Silvestre, S. Estimating the impact of azimuth-angle variations on photovoltaic annual energy production. *Clean Energy* **2019**, *3*, 47–58.

15. Abdallah, R.; Juaidi, A.; Salameh, T.; Jeguirim, M.; Çamur, H.; Kassem, Y.; Abdala, S. Estimation of solar irradiation and optimum tilt angles for south-facing surfaces in the United Arab Emirates: a case study using PVGIS and PVWatts. In *Recent Advances in*

*Renewable Energy Technologies*; Elsevier, 2022; pp. 3–39.

16.    Chang, Y.-P. Optimal the tilt angles for photovoltaic modules using PSO method with nonlinear time-varying evolution. *Energy* **2010**, *35*, 1954–1963.

17.    Dixit, T. V; Yadav, A.; Gupta, S. Annual Optimum Tilt Angle Prediction of Solar Collector using PSO Estimator. In Proceedings of the IOP Conference Series: Materials Science and Engineering; IOP Publishing, 2017; Vol. 225, p. 12296.

18.    Talebizadeh, P.; Mehrabian, M.A.; Abdolzadeh, M. Prediction of the optimum slope and surface azimuth angles using the Genetic Algorithm. *Energy Build.* **2011**, *43*, 2998–3005.

19.    Şahin, M. Determining optimum tilt angles of photovoltaic panels by using artificial neural networks in turkey. *Teh. Vjesn.* **2019**, *26*, 596–602.

20.    Yan, R.; Saha, T.K.; Meredith, P.; Goodwin, S. Analysis of yearlong performance of differently tilted photovoltaic systems in Brisbane, Australia. *Energy Convers. Manag.* **2013**, *74*, 102–108, doi:https://doi.org/10.1016/j.enconman.2013.05.007.

21.    Khasawneh, Q.A.; Damra, Q.A.; Salman, O.H.B. Determining the Optimum Tilt Angle for Solar Applications in Northern Jordan.; 2015.

22.    Darhmaoui, H.; Lahjouji, D. Latitude Based Model for Tilt Angle Optimization for Solar Collectors in the Mediterranean Region. *Energy Procedia* **2013**, *42*, 426–435, doi:https://doi.org/10.1016/j.egypro.2013.11.043.

23.    Guo, M.; Zang, H.; Gao, S.; Chen, T.; Xiao, J.; Cheng, L.; Wei, Z.; Sun, G. Optimal Tilt Angle and Orientation of Photovoltaic Modules Using HS Algorithm in Different Climates

of China. *Appl. Sci.* 2017, *7*.

24. Gong, X.; Kulkarni, M. Design optimization of a large scale rooftop photovoltaic system. *Sol. Energy* **2005**, *78*, 362–374.

25. Litjens, G.; Worrell, E.; Van Sark, W. Influence of demand patterns on the optimal orientation of photovoltaic systems. *Sol. Energy* **2017**, *155*, 1002–1014.

26. Awad, H.; Gül, M. Load-match-driven design of solar PV systems at high latitudes in the Northern hemisphere and its impact on the grid. *Sol. Energy* **2018**, *173*, 377–397, doi:https://doi.org/10.1016/j.solener.2018.07.010.

27. Liu, C.; Xu, W.; Li, A.; Sun, D.; Huo, H. Analysis and optimization of load matching in photovoltaic systems for zero energy buildings in different climate zones of China. *J. Clean. Prod.* **2019**, *238*, 117914, doi:https://doi.org/10.1016/j.jclepro.2019.117914.

28. Zhong, Q.; Tong, D. Spatial layout optimization for solar photovoltaic (PV) panel installation. *Renew. Energy* **2020**, *150*, 1–11.

29. Awan, A.B.; Alghassab, M.; Zubair, M.; Bhatti, A.R.; Uzair, M.; Abbas, G. Comparative Analysis of Ground-Mounted vs. Rooftop Photovoltaic Systems Optimized for Interrow Distance between Parallel Arrays. *Energies* **2020**, *13*, 3639.

30. Alghamdi, A.S. Performance Enhancement of Roof-Mounted Photovoltaic System: Artificial Neural Network Optimization of Ground Coverage Ratio. *Energies* **2021**, *14*, 1537.

31. Behura, A.K.; Kumar, A.; Rajak, D.K.; Pruncu, C.I.; Lamberti, L. Towards better

performances for a novel rooftop solar PV system. *Sol. Energy* **2021**, *216*, 518–529, doi:https://doi.org/10.1016/j.solener.2021.01.045.

32. Freitas, S.; Serra, F.; Brito, M.C. PV layout optimization: String tiling using a multi-objective genetic algorithm. *Sol. Energy* **2015**, *118*, 562–574.

33. Ning, G.; Junnan, L.; Yansong, D.; Zhifeng, Q.; Qingshan, J.; Weihua, G.; Geert, D. BIM-based PV system optimization and deployment. *Energy Build.* **2017**, *150*, 13–22.

34. Vahdatikhaki, F.; Salimzadeh, N.; Hammad, A. Optimization of PV modules layout on high-rise building skins using a BIM-based generative design approach. *Energy Build.* **2022**, *258*, 111787, doi:https://doi.org/10.1016/j.enbuild.2021.111787.

35. Korsavi, S.S.; Zomorodian, Z.S.; Tahsildoost, M. Energy and economic performance of rooftop PV panels in the hot and dry climate of Iran. *J. Clean. Prod.* **2018**, *174*, 1204–1214.

36. Awad, H.; Salim, K.M.E.; Gül, M. Multi-objective design of grid-tied solar photovoltaics for commercial flat rooftops using particle swarm optimization algorithm. *J. Build. Eng.* **2020**, *28*, 101080, doi:https://doi.org/10.1016/j.jobe.2019.101080.

37. Christiaanse, T. V; Loonen, R.C.G.M.; Evins, R. Techno-economic optimization for grid-friendly rooftop PV systems–A case study of commercial buildings in British Columbia. *Sustain. Energy Technol. Assessments* **2021**, *47*, 101320.

38. Mokhtara, C.; Negrou, B.; Settou, N.; Bouferrouk, A.; Yao, Y. Optimal design of grid-connected rooftop PV systems: An overview and a new approach with application to educational buildings in arid climates. *Sustain. Energy Technol. Assessments* **2021**, *47*, 101468.

39. Dubey, S.; Jadhav, N.Y.; Zakirova, B. Socio-economic and environmental impacts of silicon based photovoltaic (PV) technologies. *Energy Procedia* **2013**, *33*, 322–334.

40. Perez-Gallardo, J.R.; Azzaro-Pantel, C.; Astier, S.; Domenech, S.; Aguilar-Lasserre, A. Ecodesign of photovoltaic grid-connected systems. *Renew. Energy* **2014**, *64*, 82–97.

41. Lukač, N.; Seme, S.; Dežan, K.; Žalik, B.; Štumberger, G. Economic and environmental assessment of rooftops regarding suitability for photovoltaic systems installation based on remote sensing data. *Energy* **2016**, *107*, 854–865.

42. Allouhi, A.; Saadani, R.; Buker, M.S.; Kousksou, T.; Jamil, A.; Rahmoune, M. Energetic, economic and environmental (3E) analyses and LCOE estimation of three technologies of PV grid-connected systems under different climates. *Sol. Energy* **2019**, *178*, 25–36.

43. Cucchiella, F.; D'Adamo, I. A multicriteria analysis of photovoltaic systems: energetic, environmental, and economic assessments. *Int. J. Photoenergy* **2015**, *2015*.

44. Sagani, A.; Mihelis, J.; Dedoussis, V. Techno-economic analysis and life-cycle environmental impacts of small-scale building-integrated PV systems in Greece. *Energy Build.* **2017**, *139*, 277–290.

45. Koo, C.; Hong, T.; Park, J. Development of the life-cycle economic and environmental assessment model for establishing the optimal implementation strategy of the rooftop photovoltaic system. *Technol. Econ. Dev. Econ.* **2018**, *24*, 27–47.

46. Gómez-Navarro, T.; Brazzini, T.; Alfonso-Solar, D.; Vargas-Salgado, C. Analysis of the potential for PV rooftop prosumer production: Technical, economic and environmental assessment for the city of Valencia (Spain). *Renew. Energy* **2021**, *174*, 372–381.

47. Paudel, B.; Regmi, N.; Phuyal, P.; Neupane, D.; Hussain, M.I.; Kim, D.H.; Kafle, S. Techno-economic and environmental assessment of utilizing campus building rooftops for solar PV power generation. *Int. J. Green Energy* **2021**, 1–13.

48. Saxena, A.K.; Saxena, S.; Sudhakar, K. Energy, economic and environmental performance assessment of a grid-tied rooftop system in different cities of India based on 3E analysis. *Clean Energy* **2021**, *5*, 288–301.

49. Yıldız, G.; Çalış, B.; Gürel, A.E.; Ceylan, İ. Investigation of life cycle CO2 emissions of the polycrystalline and cadmium telluride PV panels. *Environ. Nanotechnology, Monit. Manag.* **2020**, *14*, 100343.

50. Project Sunroof Available online: https://sunroof.withgoogle.com/ (accessed on Jan 6, 2022).

51. SunPower Instant Design technology | SunPower Available online: https://us.sunpower.com/sunpower-instant-design-technology (accessed on Jan 7, 2022).

52. Solar Calculator: Estimate Solar Savings | EnergySage Available online: https://www.energysage.com/solar/calculator/ (accessed on Jan 7, 2022).

53. Solar - Mapdwell Available online: https://mapdwell.com/en/solar (accessed on Jan 7, 2022).

54. Open Buildings Available online: https://sites.research.google/open-buildings/ (accessed on Apr 19, 2022).

55. Tiwari, A.; Meir, I.A.; Karnieli, A. Object-based image procedures for assessing the solar

energy photovoltaic potential of heterogeneous rooftops using airborne LiDAR and orthophoto. *Remote Sens.* **2020**, *12*, 223, doi:https://doi.org/10.3390/rs12020223.

56.     Fuentes, J.E.; Moya, F.D.; Montoya, O.D. Method for estimating solar energy potential based on photogrammetry from unmanned aerial vehicles. *Electronics* **2020**, *9*, 2144.

57.     Nofech, J.; Narjabadifam, N.; Awad, H.; Gül, M. Mapping the solar roof potential of the North Campus buildings at the University of Alberta. In Proceedings of the 8 th Eur. Conf. Ren. Energy Sys.; 2020.

58.     Narjabadifam, N.; Al-Saffar, M.; Zhang, Y.; Nofech, J.; Cen, A.C.; Awad, H.; Versteege, M.; Gül, M. Framework for Mapping and Optimizing the Solar Rooftop Potential of Buildings in Urban Systems. *Energies* **2022**, *15*, 1738.

59.     RenderDoc Available online: https://renderdoc.org/ (accessed on Oct 31, 2021).

60.     "Blender" blender.org - Home of the Blender project - Free and Open 3D Creation Software Available online: https://www.blender.org/ (accessed on Oct 31, 2021).

61.     GitHub - eliemichel/MapsModelsImporter: A Blender add-on to import models from google maps Available online: https://github.com/eliemichel/MapsModelsImporter (accessed on Oct 31, 2021).

62.     Google Maps Available online: https://www.google.com/maps/@53.526864,-113.5241896,552m/data=!3m1!1e3 (accessed on Nov 17, 2021).

63.     Solomon, C.; Breckon, T. *Fundamentals of Digital Image Processing: A practical approach with examples in Matlab*; John Wiley & Sons, 2012;

64.    Van Den Boomgaard, R.; Van Balen, R. Methods for fast morphological image transforms using bitmapped binary images. *CVGIP Graph. Model. Image Process.* **1992**, *54*, 252–258.

65.    Sreedhar, K.; Panlal, B. Enhancement of images using morphological transformation. *arXiv Prepr. arXiv1203.2514* **2012**.

66.    Beyerer, J.; León, F.P.; Frese, C. *Machine vision: Automated visual inspection: Theory, practice and applications*; Springer, 2015; ISBN 3662477947.

67.    Duffie, J.A.; Beckman, W.A. *Solar engineering of thermal processes*; 4th ed.; John Wiley & Sons: Hoboken, New Jersey, United States of America, 2013;

68.    Awad, H. Integrating Solar PV Systems into Residential Buildings in Cold-climate Regions: The Impact of Energy-efficient Homes on Shaping the Future Smart Grid. Doctor of Philosophy, Univeristy of Alberta, Edmonton, Alberta, Canada, 2018.

69.    Badescu, V. Verification of some very simple clear and cloudy sky models to evaluate global solar irradiance. *Sol. Energy* **1997**, *61*, 251–264, doi:https://doi.org/10.1016/S0038-092X(97)00057-1.

70.    Kacira, M.; Simsek, M.; Babur, Y.; Demirkol, S. Determining optimum tilt angles and orientations of photovoltaic panels in Sanliurfa, Turkey. *Renew. energy* **2004**, *29*, 1265–1275.

71.    Bany, J.; Appelbaum, J. The effect of shading on the design of a field of solar collectors. *Sol. cells* **1987**, *20*, 201–228.

72.    EnergySage Solar Panel Size and Weight: How Big Are Solar Panels? | EnergySage

Available online: https://news.energysage.com/average-solar-panel-size-weight/ (accessed on Nov 3, 2021).

73. Bresenham, J.E. Algorithm for computer control of a digital plotter. *IBM Syst. J.* **1965**, *4*, 25–30.

74. NAIT *Alternative Energy Program Solar Photovoltaic Reference Array Report*; 2016;

75. van Vuuren, D.J.; Marnewick, A.L.; Pretorius, J.H.C. A Financial Evaluation of a Multiple Inclination, Rooftop-Mounted, Photovoltaic System Where Structured Tariffs Apply: A Case Study of a South African Shopping Centre. *Energies* **2021**, *14*, 1666.

76. Kornelakis, A.; Marinakis, Y. Contribution for optimal sizing of grid-connected PV-systems using PSO. *Renew. Energy* **2010**, *35*, 1333–1341.

77. Dağtekin, M.; Kaya, D.; Öztürk, H.H.; Kiliç, F.Ç. A study of techno-economic feasibility analysis of solar photovoltaic (PV) power generation in the province of Adana in Turkey. *Energy Explor. Exploit.* **2014**, *32*, 719–735.

78. Thebault, M.; Gaillard, L. Optimization of the integration of photovoltaic systems on buildings for self-consumption–Case study in France. *City Environ. Interact.* **2021**, *10*, 100057.

79. White, J.A.; Grasman, K.S.; Case, K.E.; Needy, K.L.; Pratt, D.B. *Fundamentals of engineering economic analysis*; John Wiley & Sons, 2020; ISBN 1118881060.

80. U.S. Energy Information Administration (EIA) Available online: https://www.eia.gov/tools/faqs/faq.php?id=74&t=11 (accessed on Jan 21, 2022).

81. NREL Life Cycle Greenhouse Gas Emissions from Solar Photovoltaics (Fact Sheet), NREL (National Renewable Energy Laboratory) 2012.

82. Makrides, G.; Zinsser, B.; Phinikarides, A.; Schubert, M.; Georghiou, G.E. Temperature and thermal annealing effects on different photovoltaic technologies. *Renew. Energy* **2012**, *43*, 407–417.

83. CanadianSolar Datasheet Available online: https://static.csisolar.com/wp-content/uploads/2019/12/07162836/CS-Datasheet-HiKu_CS3W-P_EN.pdf (accessed on Jun 21, 2021).

84. Micro-Generation in Alberta – EnergyRates.ca Available online: https://energyrates.ca/alberta/micro-generation-in-alberta/ (accessed on Nov 8, 2021).

85. Budget 2020 : a plan for jobs and the economy - Open Government Available online: https://open.alberta.ca/dataset/budget-2020 (accessed on Oct 1, 2021).

86. POWER | Data Access Viewer Available online: https://power.larc.nasa.gov/data-access-viewer/ (accessed on Aug 10, 2021).

87. PVWatts Calculator Available online: https://pvwatts.nrel.gov/pvwatts.php (accessed on Oct 1, 2021).

88. Residential and Commercial Solar Program in Alberta Available online: https://alberta-solar-installers.ca/program-types/residential-and-commercial-solar-program-in-alberta (accessed on Nov 13, 2021).

89. Residential and Commercial Solar Program – EnergyRates.ca Available online:

https://energyrates.ca/alberta/residential-commercial-solar-program/ (accessed on Nov 13, 2021).